Cross-Section Parameterizations for Pion and Nucleon Production From Negative Pion-Proton Collisions

John W. Norbury, Steve R. Blattnig, and Ryan Norman
University of Wisconsin-Milwaukee, Milwaukee, Wisconsin

R. K. Tripathi
Langley Research Center, Hampton, Virginia

December 2002

The NASA STI Program Office . . . in Profile

Since its founding, NASA has been dedicated to the advancement of aeronautics and space science. The NASA Scientific and Technical Information (STI) Program Office plays a key part in helping NASA maintain this important role.

The NASA STI Program Office is operated by Langley Research Center, the lead center for NASA's scientific and technical information. The NASA STI Program Office provides access to the NASA STI Database, the largest collection of aeronautical and space science STI in the world. The Program Office is also NASA's institutional mechanism for disseminating the results of its research and development activities. These results are published by NASA in the NASA STI Report Series, which includes the following report types:

- TECHNICAL PUBLICATION. Reports of completed research or a major significant phase of research that present the results of NASA programs and include extensive data or theoretical analysis. Includes compilations of significant scientific and technical data and information deemed to be of continuing reference value. NASA counterpart of peer-reviewed formal professional papers, but having less stringent limitations on manuscript length and extent of graphic presentations.

- TECHNICAL MEMORANDUM. Scientific and technical findings that are preliminary or of specialized interest, e.g., quick release reports, working papers, and bibliographies that contain minimal annotation. Does not contain extensive analysis.

- CONTRACTOR REPORT. Scientific and technical findings by NASA-sponsored contractors and grantees.

- CONFERENCE PUBLICATION. Collected papers from scientific and technical conferences, symposia, seminars, or other meetings sponsored or co-sponsored by NASA.

- SPECIAL PUBLICATION. Scientific, technical, or historical information from NASA programs, projects, and missions, often concerned with subjects having substantial public interest.

TECHNICAL TRANSLATION. English-language translations of foreign scientific and technical material pertinent to NASA's mission.

Specialized services that complement the STI Program Office's diverse offerings include creating custom thesauri, building customized databases, organizing and publishing research results . . . even providing videos.

For more information about the NASA STI Program Office, see the following:

- Access the NASA STI Program Home Page at *http://www.sti.nasa.gov*

- Email your question via the Internet to help@sti.nasa.gov

- Fax your question to the NASA STI Help Desk at (301) 621-0134

- Telephone the NASA STI Help Desk at (301) 621-0390

- Write to:
  NASA STI Help Desk
  NASA Center for AeroSpace Information
  7121 Standard Drive
  Hanover, MD 21076-1320

NASA/TP-2002-211766

Cross-Section Parameterizations for Pion and Nucleon Production From Negative Pion-Proton Collisions

John W. Norbury, Steve R. Blattnig, and Ryan Norman
University of Wisconsin-Milwaukee, Milwaukee, Wisconsin

R. K. Tripathi
Langley Research Center, Hampton, Virginia

December 2002

Acknowledgments

Nomenclature

Note: the units used in this work are such that $\hbar = c = 1$.

1	symbol for projectile particle in the reaction $1 + 2 \rightarrow$ anything
2	symbol for target particle in the reaction $1 + 2 \rightarrow$ anything
cm	symbol for center of momentum frame, where $\mathbf{p}_1 + \mathbf{p}_2 = 0$
lab	symbol for lab (target) frame, where $\mathbf{p}_2 = 0$
x^*	denotes a variable x in the cm frame
x_{lab}	denotes a variable x in the lab frame
x	denotes a variable x in the lab frame or denotes an invariant variable x
π	symbol for pion (either π^0, π^+, or π^-)
N	symbol for nucleon (either proton or neutron)
n	symbol for neutron
p	symbol for proton
	Note: not to be confused with magnitude of momentum. Context will make clear.
m_π	pion mass, GeV
m_p	proton mass, GeV
m_i	mass of particle i, GeV
T	particle kinetic energy, GeV
E	particle total energy, GeV
p	magnitude of 3-momentum, $p = |\mathbf{p}|$, GeV
	Note: not to be confused with symbol for proton. Context will make clear.
β	speed of cm frame
γ	relativistic γ factor, $\gamma = \frac{1}{\sqrt{1-\beta^2}}$
$\frac{d^3\sigma}{dp^3/E}$	Lorentz invariant differential cross section, mb/GeV^2
$\frac{d\sigma}{dE}$	spectral distribution cross section, mb/GeV
σ	total cross section, mb
$\frac{d^2N}{dp_\| dp_\perp}$	single particle distribution in the projectile-nucleon cm frame
$\sqrt{s}$	total energy in cm frame, $E_{1\,cm} + E_{2\,cm} \equiv E_{cm}$, GeV
$\mathbf{p}_\pi^{*2}$	pion momentum in cm frame, GeV
$\mathbf{p}_{\pi\,\text{max}}^{*2}$	maximum pion momentum in cm frame, GeV
$\theta_{\pi\,\text{max}}$	maximum pion angle in lab frame
$p_{1\,\text{lab}}$	magnitude of 3-momentum of particle 1 in lab frame for reaction $1 + 2 \rightarrow 3 + 4$, $|\mathbf{p}|_{1\,\text{lab}}$, GeV
$E_{1\,lab}$	total energy of particle 1 in the lab frame for the reaction $1 + 2 \rightarrow 3 + 4$, $\sqrt{|\mathbf{p}|_{1\,lab}^2 + m_1^2}$, GeV
p_t	transverse momentum, GeV
p^μ	4-momentum vector, $p^\mu = (E, \mathbf{p})$, GeV
$(p^\mu)^2$	square of 4-momentum vector, $(p^\mu)^2 = E^2 - \mathbf{p}^2 = m^2$, GeV^2
p_i^μ	4-momentum vector of particle i, GeV

Abstract

Ranft has provided parameterizations of Lorentz invariant differential cross sections for pion and nucleon production in pion-proton collisions that are compared to some recent data. The Ranft parameterizations are then numerically integrated to form spectral and total cross sections. These numerical integrations are further parameterized to provide formulas for spectral and total cross sections suitable for use in radiation transport codes. The reactions that are analysed are for charged pions in the initial state and for both charged and neutral pions in the final state.

1. Introduction

The development of the HZETRN code (refs. 1–4) which predicts space radiation environments, has reached the stage where meson interactions need to be considered. The lightest meson is the pion and is therefore the most important one from a radiation point of view. The next lightest meson is the kaon, and its interactions will be dealt with in future work. For the present, only pion interactions will be considered.

Previous work (refs. 5–8) evaluated pion production in proton-proton collisions. The π^0 decays electromagnetically with a lifetime of $\tau = 8.4 \times 10^{-17}$sec that corresponds to a decay length $c\tau = 25.1$ nm. This short decay length means, from a radiation transport point of view, that it can be considered to decay instantaneously. Thus, for the HZETRN code, the π^0 does not propagate, and its interactions with the target constituents do not need to be considered.

On the other hand, the charged pions, π^+ and π^-, decay weakly and therefore have a much longer lifetime and longer decay length. The lifetime is $\tau = 2.6 \times 10^{-8}$sec that corresponds to a decay length $c\tau = 7.8$ m. This long decay length means that charged pion propagation needs to be included in HZETRN because the pions will interact with target materials before they decay. From this point of view, it is very interesting that the Weak interaction has an extremely important role in space radiation transport applications.

The present work involves the interaction of these charged pions with the protons in the target material. The final states considered will be pion production and proton production. HZETRN requires spectral distributions in the lab (target) frame as well as total cross sections. Parameterizations of these cross sections will be developed as will parameterizations of the Lorentz invariant differential cross sections. (These latter parameterizations will be useful when developing angular distributions for later use in a 3-dimensional transport code.)

Analysis of the relevant pion reactions has been extensively discussed in reference 9. All possible Strong exclusive reactions were itemized, along with thresholds and mass values of the set of inclusive particles for the minimum threshold reactions. These results (ref. 9) are used in the present work, especially in doing numerical integrations.

Appendices A–D contain the following information: appendix A presents data that relates to Lorentz transformations; appendix B has useful kinetic results; appendix C presents data about maximum pion momentum in the cm frame, and appendix D contains data regarding the maximum pion angle in the lab frame.

The threshold energies are derived in reference 9. Because of the method used to parameterize cross sections (refs. 5–9), the threshold does not appear automatically in the parameterizations. When putting cross sections into a code like HZETRN, it is important to include a code statement that will set the cross section to zero when the energy is below threshold.

2. Ranft Parameterizations of Lorentz Invariant Differential Cross Section for Pion-Proton Collisions

Ranft (ref. 10) provides parameterizations of the single particle distributions, $\frac{d^2N}{dp_{||}dp_\perp}$ which are related to the Lorentz invariant differential cross section according to

$$\frac{d^2\sigma}{dp_{||}dp_\perp} = \sigma_{\text{inelastic}}\frac{d^2N}{dp_{||}dp_\perp} \tag{1}$$

The total inelastic cross section (ref. 10) rises approximately as $A^{2/3}$. For pion-nucleus collisions, Ranft (ref. 10) uses

$$\sigma_{\text{inelastic}} = 28.5A^{0.73} \tag{2}$$

where $A = 1$ for the pion-proton reactions considered in the present work. This value of $\sigma_{\text{inelastic}}$ is used in both of the following subsections for pion and nucleon (proton or neutron) production from pion-proton collisions.

We require the Lorentz invariant differential cross section $\frac{d^3\sigma}{dp^3/E} = E\frac{d^3\sigma}{dp^3}$ where $E \equiv E_\pi$ is the pion total energy and $p \equiv |\mathbf{p}_\pi|$ is the magnitude of the pion 3-momentum. The 3-momentum volume element is

$$\begin{aligned}
dp^3 &= p^2dpd\Omega = 2\pi p^2dp\sin\theta d\theta \quad \text{(in spherical coordinates)} \tag{3}\\
&= 2\pi dp_{||}p_\perp dp_\perp = \pi dp_{||}dp_\perp^2 \quad \text{(in cylindrical coordinates)} \tag{4}
\end{aligned}$$

We want the relation between $\frac{d^3\sigma}{dp^3/E}$ and $\frac{d^2\sigma}{dp_\parallel dp_\perp}$. Thus,

$$\frac{d^3\sigma}{dp^3/E} = \frac{E}{2\pi p_\perp}\frac{d^2\sigma}{dp_\parallel dp_\perp} \tag{5}$$

$$= \sigma_{\text{inelastic}}\frac{E}{2\pi p_\perp}\frac{d^2N}{dp_\parallel dp_\perp} \tag{6}$$

2.1 Pion Production

This subsection considers the reactions

$$\pi + p \rightarrow \pi + X \tag{7}$$

Ranft (ref. 10) has parameterized the single particle pion distributions as

$$\frac{d^2N}{dp_\parallel dp_\perp} = \left[a_5\exp(-4\frac{a_6}{s}p_\parallel^2) + a_7\right]a_8^2\, p_\perp\frac{\exp(-a_8 p_\perp)}{E_\pi} \qquad \text{for } p_\parallel < 0 \quad (\text{i.e. } \theta > 90^o) \tag{8}$$

and

$$\frac{d^2N}{dp_\parallel dp_\perp} = \left[a_1\exp(-4\frac{a_2}{s}p_\parallel^2) + a_3\right]a_4^2\, p_\perp\frac{\exp(-a_4 p_\perp)}{E_\pi} \qquad \text{for } p_\parallel > 0 \quad (\text{i.e. } \theta < 90^o) \tag{9}$$

where $p_\perp$ and $p_\parallel$ refer to the final state pion produced and where $s \equiv E_{cm}^2$ and $E_\pi^2 \equiv p_\parallel^2 + p_\perp^2 + m_\pi^2 = p^2 + m_\pi^2$. (Note that Ranft incorrectly writes $p_\parallel > 0$ for both of the above formulas.) The Ranft parameters for pion production are listed in table 1.

Table 1. Parameters for Equations (8) and (9) or (10) and (11)

Reaction	a_1	a_2	a_3	a_4	a_5	a_6	a_7	a_8
$\pi^+ + p \rightarrow \pi^+ + X$	0.22	7	0	5.7	0.22	5	0.115	5.7
$\pi^+ + p \rightarrow \pi^0 + X$ $\pi^+ + p \rightarrow \pi^- + X$ $\pi^- + p \rightarrow \pi^0 + X$ $\pi^- + p \rightarrow \pi^+ + X$	$0.14 - 0.14/\sqrt{s}$	13	0	5.7	$0.14 - 0.14/\sqrt{s}$	9	0	5.7
$\pi^- + p \rightarrow \pi^- + X$	0.22	7	0	5.7	0.22	5	0.115	5.7

Substituting the Ranft parameterizations for $\frac{d^2N}{dp_\parallel dp_\perp}$ gives

$$\frac{d^3\sigma}{dp^3/E} = \sigma_{\text{inelastic}}\frac{a_8^2}{2\pi}\left[a_5\exp(-4\frac{a_6}{s}p_\parallel^2) + a_7\right]\exp(-a_8 p_\perp)$$
$$\text{for } p_\parallel < 0 \quad (\text{i.e., } \theta > 90^o) \tag{10}$$

3

and

$$\frac{d^3\sigma}{dp^3/E} = \sigma_{\text{inelastic}} \frac{a_4^2}{2\pi} \left[a_1 \exp(-4\frac{a_2}{s}p_{||}^2) + a_3 \right] \exp(-a_4 p_\perp)$$

$$\text{for } p_{||} > 0 \quad (\text{i.e., } \theta < 90^o) \tag{11}$$

where $E \equiv E_\pi$ and p^3, $p_{||}$ and $p_\perp$ are also all final state pion variables.

These parameterizations are compared to data in figures 1–10. Clearly the Ranft parameterization provides a poor fit to the data.

2.2 Nucleon Production

This subsection considers the reactions

$$\pi + p \rightarrow N + X \tag{12}$$

where N is either a proton (p) or neutron (n).

Ranft (ref. 10) has parameterized the single particle nucleon (proton or neutron) distributions as

$$\frac{d^2N}{dp_{||}dp_\perp} = \frac{a_1}{\sqrt{s}} \left(1 + \frac{a_2}{\sqrt{s}}p_{||} + \frac{a_3}{s}p_{||}^2\right) p_\perp \left[\exp(-a_4 p_\perp^2) + a_5 \exp(-a_6 p_\perp)\right]$$

$$\text{for } p_{||} < 0 \quad (\text{i.e. } \theta > 90^o) \tag{13}$$

and

$$\frac{d^2N}{dp_{||}dp_\perp} = 0 \qquad \text{for } p_{||} > 0 \quad (\text{i.e. } \theta < 90^o) \tag{14}$$

where $p_\perp$ and $p_{||}$ refer to the final state nucleon produced. The Ranft parameters for nucleon production are listed in table 2.

However, these parameterizations cannot possibly be right as the data (ref. 11) show a large cross section for $\theta < 90^o$ and a smaller, non-zero cross section for $\theta > 90^o$. Thus, for the rest of this section and in figures 10 – 15, the Ranft parameterization is herein defined as equation (13). Thus, we define the Ranft parameterization for nucleon production as

$$\frac{d^2N}{dp_{||}dp_\perp} = \frac{a_1}{\sqrt{s}} \left(1 + \frac{a_2}{\sqrt{s}}p_{||} + \frac{a_3}{s}p_{||}^2\right) p_\perp \left[\exp(-a_4 p_\perp^2) + a_5 \exp(-a_6 p_\perp)\right] \tag{15}$$

irrespective of the angle. (Note that in the end, these details really do not matter because we will be developing our own parameterizations to be used in the transport codes, and the end results do not depend on how the Ranft parameterization is defined.)

4

Table 2. Parameters for Equations (13) and (14) or (15) and (16)
(The numbers are the same for all reactions listed.)

Reaction	a_1	a_2	a_3	a_4	a_5	a_6
$\pi^+ + p \rightarrow p + X$						
$\pi^+ + p \rightarrow n + X$	0.94	0.86	-3.37	3.78	0.47	3.6
$\pi^- + p \rightarrow p + X$						
$\pi^- + p \rightarrow n + X$						

Substituting the Ranft parameterizations for $\frac{d^2N}{dp_\parallel dp_\perp}$ gives

$$\frac{d^3\sigma}{dp^3/E} = \sigma_{\text{inelastic}} \frac{Ea_1}{2\pi\sqrt{s}} \left(1 + \frac{a_2}{\sqrt{s}}p_\parallel + \frac{a_3}{s}p_\parallel^2\right) \left[\exp(-a_4 p_\perp^2) + a_5 \exp(-a_6 p_\perp)\right] \qquad (16)$$

where $E \equiv E_N$ and p^3, $p_\parallel$ and $p_\perp$ are also all final state nucleon variables.

These parameterizations are compared to data in figures 11 – 15. Clearly the Ranft parameterization provides a poor fit to the data.

3. New Parameterizations of Lorentz Invariant Differential Cross Section for Pion-Proton Collisions

Due to the poor fit of the Ranft parameterizations compared to the data, new parameterizations were developed, as described below. They are compared to the Ranft parameterizations in figures 1 – 15.

3.1 Pion Production

The new parameterizations for pion production in the present work are

$$\frac{d^3\sigma}{dp^3/E} = N\sigma_{\text{inelastic}} \frac{a_8^2}{2\pi} \left[a_5 \exp(-4\frac{a_6}{s}p_\parallel^2) + a_7\right] \exp(-a_8 p_\perp^{pp})$$
$$\text{for } p_\parallel < 0 \quad (\text{i.e., } \theta > 90^o) \qquad (17)$$

and

$$\frac{d^3\sigma}{dp^3/E} = N\sigma_{\text{inelastic}} \frac{a_4^2}{2\pi} \left[a_1 \exp(-4\frac{a_2}{s}p_\parallel^2) + a_3\right] \exp(-a_4 p_\perp^{pp})$$
$$\text{for } p_\parallel > 0 \quad (\text{i.e., } \theta < 90^o) \qquad (18)$$

with $N = 2$ and $pp = 0.95$. The parameters $a_1 \cdots a_8$ are the same as listed previously in table 1.

5

3.2 Nucleon Production

A major problem with the Ranft parameterization is that the value of the parameter a_3 is negative, as shown in table 2, and sometimes leads to negative cross sections, which is disastrous when integrating to form spectral and total cross sections. In addition, the Ranft parameterization blows up for large $p_{||}$, which is also a disaster when integrating.

A new parameterization using the pion parameters for π^+ production was used. It is the same as the new π^+ parameterization mentioned previously except that $N = 2$ and $pp = 0.9$. Also, where m_π appears in the pion parameterization, m_p is used here instead.

As can be seen in figures 1 – 15, the new parameterizations for pion and proton production provide a much better fit to the data.

4. Parameterization of Spectral Distribution

The spectral distribution $\frac{d\sigma}{dE}$ is related to the Lorentz invariant differential cross section by references 5 and 6.

$$\frac{d\sigma}{dE} = 2\pi p \int_0^{\theta_{max}} \frac{d^3\sigma}{dp^3/E} \; \sin\theta d\theta \tag{19}$$

If $\frac{d^3\sigma}{dp^3/E}$ is given in the *cm* frame, then one simply performs the numerical integration to obtain $\frac{d\sigma}{dE}$ in the *cm* frame. (In the *cm* frame $\theta_{max} \equiv \theta^*_{max} = \pi$.) However things are not this simple. The parameterizations for $\frac{d^3\sigma}{dp^3/E}$ of Badhwar (ref. 12), Badhwar and Stephens (ref. 13), and Ranft (ref. 10) are given in the *cm* frame, but the HZETRN code (refs. 1–4) requires $\frac{d\sigma}{dE}$ in the lab frame. To achieve the compatibility of the frames one integrates over lab frame variables. One must specify E or $|\mathbf{p}|$ and θ in the lab frame and obtain E^* or $|\mathbf{p}^*|$ and θ^* in the *cm* frame by using equations (41) and (42). These *cm* variables are input into the formula (parameterization) for $\frac{d^3\sigma}{dp^3/E}$. Because $\frac{d^3\sigma}{dp^3/E}$ is Lorentz invariant, the number so obtained will also be the value of $\frac{d^3\sigma}{dp^3/E}$ in the lab frame. Thus, this procedure gives $\frac{d\sigma}{dE}$ in the lab frame. A complication is that $\theta_{\max}$ must be determined in the lab frame. This transformation is discussed in appendix D.

4.1 Parameterizations

The new parameterizations of the Lorentz invariant differential cross section were numerically integrated over angle, as described above, and then functions were fit to this numerical data. The following functions were found to best fit the π production data, as

shown in figures 16 – 25. The resulting parameterization of the spectral distributions in the lab frame:

$$\frac{d\sigma}{dE} = 32.5 \, \text{Log}[\text{p}_{1\,\text{lab}}] \exp[-\text{p}_{1\,\text{lab}}^{0.2}] \frac{(\text{E} - \text{m}_\pi)^{0.05}}{\text{E}^{0.4}} \exp[-\text{E}^{0.5}] \text{ for } \pi^+ \text{ production} \quad (20)$$

$$= 60.6 \, \text{Log}[\text{p}_{1\,\text{lab}}] \exp[-\text{p}_{1\,\text{lab}}^{0.2}] \frac{(\text{E} - \text{m}_\pi)^{0.05}}{\text{E}^{0.4}} \exp[-\text{E}^{0.5}] \text{ for } \pi^- \text{ production} \quad (21)$$

Note that the cross section units are in mb/GeV and all energies are in GeV; E is the total energy (E=T+m) of the produced particle. Actually, the technique used was first to fit the total cross section, as described below, because doing so gives one a good idea of the $p_{1\,\text{lab}}$ dependence.

The proton production spectral distributions were much more difficult to fit. The difficulty was in obtaining the $p_{1\,\text{lab}}$ dependence. The best method found was to fit each spectral distribution separately at the $p_{1\,\text{lab}}$ values of 2, 5, 10, 50, and 100 GeV as shown in figures 26 – 30. The spectral distributions for the regions in between these $p_{1\,\text{lab}}$ values are well approximated by the previous $p_{1\,\text{lab}}$ fits. For example, the spectral distribution at 7.5 GeV is well approximated by the fitted spectral distribution at 5 GeV. Similarly, the spectral distribution at 75 GeV is well approximated by the fitted spectral distribution at 50 GeV. Thus, the parameterization developed for the proton production spectral distributions are

$$\frac{d\sigma}{dE} = \exp[a2 + (b2 * \text{E}^3) + (c2/\text{E}) + (d2/\text{E}^{1.5})] \qquad \text{for } \text{p}_{1\,\text{lab}} \leq 2.5 \text{ GeV}$$

$$= \exp[a5 + b5 * \text{E}^{1.5} + c5/\text{E}^2] \qquad \text{for } \text{p}_{1\,\text{lab}} \leq 7.5 \text{ GeV}$$

$$= \exp[a10 + b10 * \text{E}^3 + c10 * (\text{Log}[\text{E}]/\text{E})] \qquad \text{for } \text{p}_{1\,\text{lab}} \leq 25 \text{ GeV}$$

$$= a50 + b50 * E + c50 * (\text{Log}[\text{E}]/\text{E}) + (d50/\text{E})$$
$$\quad + e50/E^{1.5} + f50 * (\text{Log}[\text{E}]/\text{E}^2) + g50 * \exp[-\text{E}] \quad \text{for } \text{p}_{1\,\text{lab}} \leq 75 \text{ GeV}$$

$$= a100 + b100 * E + c100 * (\text{Log}[\text{E}]/\text{E})$$
$$\quad + d100/E + (e100/E^{1.5}) + f100/E^2 \qquad \text{for } \text{p}_{1\,\text{lab}} > 75\text{GeV} \quad (22)$$

The parameter values are:
$a2 = -21.719014$, $b2 = -0.010239021$, $c2 = 120.40895$, $d2 = -110.09389$, $a5 = 3.8409577$, $b5 = -0.75010595$, $c5 = -8.2109936$, $a10 = -4.9989318$, $b10 = -0.00873275$, $c10 = 12.995241$, $a50 = -0.2800469$, $b50 = 0.0066378301$, $c50 = -5.6547689$, $d50 = 27.961949$, $e50 = -28.032802$, $f50 = -9.3283952$, $g50 = 0.93580082$, $a100 = 0.66853886$, $b100 = -0.0097222382$, $c100 = -16.638858$, $d100 = 61.302023$, $e100 = -93.829375$, and $f100 = 31.86854$.

The results of the "in-between" $p_{1\,\text{lab}}$ values are shown in figures 31 – 35. It can be seen that the results are excellent.

5. Parameterization of Total Cross Section

5.1 Spherical Coordinates

The total cross section σ is related to the spectral distribution cross section by

$$\sigma = \int \frac{d\sigma}{dE} dE = \int \frac{d\sigma}{dE} \frac{p}{E} dp \tag{23}$$

where $E \equiv \sqrt{p^2 + m^2}$ and $p \equiv |\mathbf{p}|$. Thus, the relation to the Lorentz invariant differential cross section is (ref. 6)

$$\sigma = 2\pi \int_0^{\theta_{\max}} d\theta \int_{p_{\min}}^{p_{\max}} dp \, \frac{d^3\sigma}{dp^3/E} \frac{p^2 \sin\theta}{\sqrt{p^2 + m^2}} \tag{24}$$

There are two ways to calculate σ. One can work in either the cm or lab frame because σ is Lorentz invariant.

The simplest thing is to do the entire double integration in the cm frame. In that case, $\theta^*_{\max} = \pi$ $p^*_{\min} = 0$ and $p^*_{\max}$ is discussed in appendix C. By checking that the same result is obtained, one could also continue calculating in the lab frame, as was the case with the spectral distribution discussed previously. The value of $\theta_{\max \, \text{lab}}$ is discussed in appendix D; $p^*_{\max}$, discussed in appendix C, and $p^*_{\min} = 0$ must both be transformed to the lab frame. The value of $p_{\min \, \text{lab}}$ will not necessarily be zero.

5.2 Cylindrical Coordinates

The parameterizations of the Lorentz invariant differential cross sections of Badhwar, Badhwar and Stephens (refs. 12 and 13) and Ranft (ref. 10) are not only given in the cm frame but are also written in terms of cylindrical coordinates $(p_\perp, p_\parallel)$ rather than the spherical coordinates $(|\mathbf{p}|, \theta)$. Thus, it is always worth trying to do the integrations in cylindrical rather than with spherical coordinates because the integrals may be able to be done analytically. Unfortunately, to obtain the spectral distribution $\frac{d\sigma}{dE}$, this approach is impossible because E is intrinsically a spherical coordinate. A single integral over $\int dp_\parallel$ will yield $\frac{d\sigma}{dp_\perp}$, or an integral over $\int dp_\perp$ will yield $\frac{d\sigma}{dp_\parallel}$, but neither $\frac{d\sigma}{dp_\perp}$ or $\frac{d\sigma}{dp_\parallel}$ will yield $\frac{d\sigma}{dE}$ exactly, which is what we seek ($\frac{d\sigma}{dp_\parallel}$ can however yield $\frac{d\sigma}{dE}$ approximately (refs. 7 and 8)).

Nevertheless, both spherical and cylindrical coordinate integration will yield the total cross section σ exactly. Thus, it is an excellent check of one's work to calculate the total cross section by using both coordinate systems. Obviously

$$\sigma = \int \frac{d^2\sigma}{dp_\parallel dp_\perp} dp_\parallel dp_\perp \tag{25}$$

Using equation (5), this gives

$$\sigma = 2\pi \int dp_{\parallel} \; \int dp_{\perp} \; \frac{d^3\sigma}{dp^3/E} \; \frac{p_{\perp}}{\sqrt{p_{\parallel}^2 + p_{\perp}^2 + m^2}} \tag{26}$$

with $E = \sqrt{p_{\parallel}^2 + p_{\perp}^2 + m^2}$.

Again, this integral can be done in either the *cm* or lab frames; however, given that the original parameterizations (refs. 10, 12, and 13) are in the *cm* frame, it makes sense to do the double integral in this frame.

The question then arises as to the integration limits. The lower limit of $p \equiv |\mathbf{p}|$ in the *cm* frame is zero, and so obviously the lower limits of $p_{\parallel}$ and $p_{\perp}$ will also be zero. For the upper limit, consider the result of appendix C, where $p_{\max}$ was determined in spherical coordinates. Given that $p_{\parallel} = p \sin\theta$ and $p_{\perp} = p \cos\theta$, obviously the upper limits of $p_{\parallel}$ and $p_{\perp}$ occur when $\sin\theta$ or $\cos\theta$ equals unity. Thus, the upper limits of $p_{\parallel}$ and $p_{\perp}$ will be the same as the spherical case, namely the exact result derived in appendix C. Thus the final formula, working in the *cm* frame, is

$$\sigma = 2\pi \int_0^{p_{\max}^*} dp_{\parallel} \; \int_0^{p_{\max}^*} dp_{\perp} \; \frac{d^3\sigma}{dp^3/E} \; \frac{p_{\perp}}{\sqrt{p_{\parallel}^2 + p_{\perp}^2 + m^2}} \tag{27}$$

where $p_{\max}^* = |\mathbf{p}_{\max}^*|$ from appendix C.

5.3 Parameterizations

The new parameterizations of the Lorentz invariant differential cross section were numerically integrated over energy and angle, as described previously, and then functions were fit to this numerical data. The following functions were found to best fit the data, as shown in figures 36 – 38.

$$
\begin{aligned}
\sigma & = & 6.5 \, \text{Log}[\text{p}_{1\,\text{lab}}] & \qquad \text{for } \pi^+ \text{ production} & (28) \\
& = & 10.1 \, \text{Log}[\text{p}_{1\,\text{lab}}] & \qquad \text{for } \pi^- \text{ production} & (29) \\
& = & 0.5 \, \text{Log}[\text{p}_{1\,\text{lab}}]\text{p}_{1\,\text{lab}}^{0.17} & \qquad \text{for p production} & (30)
\end{aligned}
$$

Note that the cross section units are in mb.

6. Conclusions

Ranft has provided parameterizations of Lorentz invariant differential cross sections for pion and nucleon production in pion-proton collisions. These parameterizations have been

compared to some recent data. The reactions analysed are for charged pions in the initial state and for both charged and neutral pions in the final state at an incident pion energy of 40 GeV. The present work has shown some inadequacies in the Ranft parameterizations, and it is therefore recommended to use the parameterizations developed herein for energies in the 1–100 GeV range.

Appendix A

Lorentz Transformations

In the typical scenario discussed in the present paper, all variables shown subsequently refer to the pion; e.g., $E \equiv E_\pi$, $p \equiv p_\pi$, $\theta \equiv \theta_\pi$ and so on. Variables with a star * refer to cm variables; while variables without a star are lab variables. Thus, for example, θ is the angle of the pion in the lab frame, and θ^* is the angle of the pion in the cm frame. Exceptions are β and γ which refer to the speed of the cm frame relative to the lab.

In this appendix, the Lorentz transformations that will be needed are summarized. First, define the perpendicular (transverse) and parallel momenta as

$$\begin{aligned} p_\perp &\equiv p\sin\theta \\ p_\parallel &\equiv p\cos\theta \end{aligned} \tag{31}$$

where

$$p \equiv |\mathbf{p}|$$

The total energy is

$$E = T + m = \sqrt{p^2 + m^2} = \sqrt{p_\perp^2 + p_\parallel^2 + m^2} \tag{32}$$

The Lorentz transformation of 4-momenta $p^\mu = (E, \mathbf{p})$ from cm to lab frame, assuming relative motion in the parallel direction, is given by Barnett (ref. 16):

$$p_\perp = p_\perp^*$$

$$\begin{pmatrix} E \\ p_\parallel \end{pmatrix} = \begin{pmatrix} \gamma & \gamma\beta \\ \gamma\beta & \gamma \end{pmatrix} \begin{pmatrix} E^* \\ p_\parallel^* \end{pmatrix} \tag{33}$$

where β is the speed of the cm relative to the lab frame and $\gamma = \frac{1}{\sqrt{1-\beta^2}}$. Thus, $p \equiv |\mathbf{p}|$ transforms as

$$p \equiv \sqrt{p_\perp^2 + p_\parallel^2} = \sqrt{(p^*\sin\theta^*)^2 + (\gamma\beta E^* + \gamma p^*\cos\theta^*)^2} \tag{34}$$

An important quantity is the Lorentz transformation of the pion angle. Obviously,

$$\tan\theta = \frac{p_\perp}{p_\parallel} = \frac{p_\perp^*}{\gamma\beta E^* + \gamma p_\parallel^*} = \frac{p^*\sin\theta^*}{\gamma\beta E^* + \gamma p^*\cos\theta^*} \tag{35}$$

This equation can also be written (see ref. 14) as

$$
\begin{aligned}
\tan\theta &= \frac{p^* \sin\theta^*}{\gamma\beta E^* + \gamma p^* \cos\theta^*} \\
&= \frac{E^* \sin\theta^*}{(E_{1\,\text{lab}} + m_2)(\cos\theta^* + \alpha)}
\end{aligned}
\tag{36}
$$

with α being the ratio of the cm speed to the speed of particle 3 in the cm system (ref. 14),

$$
\alpha \equiv \frac{\beta E^*}{p^*}
\tag{37}
$$

For the reaction, with a 2-body final state,

$$
1 + 2 \to 3 + 4
$$

there is a unique relationship between the angles and momenta of the emerging particles (ref. 15), so that α is also equal to (ref. 14)

$$
\alpha \equiv \frac{\beta E^*}{p^*} = \left(\frac{p_{1\,\text{lab}}}{E_{1\,\text{lab}} + m_2}\right) \frac{s + m_3^2 - m_4^2}{[s - (m_3 + m_4)^2][s - (m_3 - m_4)^2]}
\tag{38}
$$

If three or more particles emerge in the final state, then there are no longer unique relationships but only limiting relationships (ref. 15). For the inclusive reaction

$$
1 + 2 \to 3 + X
\tag{39}
$$

where X is anything, including many other particles, $X = 4, 5, 6...$, then only equation (37) holds. The second equality in equation (38) does not hold for the inclusive reaction of equation (39). (The second equality would only hold if we knew all the masses and set m_4 equal to the masses of all the particles X.)

The inverse transformation from lab to cm is obtained by swapping starred and un-starred quantities and changing the sign of the speed β, giving

$$
p_\perp^* = p_\perp
$$

$$
\begin{pmatrix} E^* \\ p_\parallel^* \end{pmatrix} = \begin{pmatrix} \gamma & -\gamma\beta \\ -\gamma\beta & \gamma \end{pmatrix} \begin{pmatrix} E \\ p_\parallel \end{pmatrix}
\tag{40}
$$

p transforms as

$$
p^* = \sqrt{(p\sin\theta)^2 + (-\gamma\beta E + \gamma p\cos\theta)^2}
\tag{41}
$$

The inverse angle transformation is

$$
\tan\theta^* = \frac{p_\perp^*}{p_\parallel^*} = \frac{p_\perp}{-\gamma\beta E + \gamma p_\parallel} = \frac{p\sin\theta}{-\gamma\beta E + \gamma p\cos\theta}
\tag{42}
$$

12

Appendix B

Useful Kinematic Results

Relation Between s and Total cm Energy

The 4-momentum vector p^μ is

$$p^\mu = (E, \mathbf{p}) \tag{43}$$

with the square given by

$$(p^\mu)^2 = E^2 - \mathbf{p}^2 = m^2 \tag{44}$$

showing that the square of this 4-vector is invariant. For the reaction

$$1 + 2 \to 3 + 4$$

the Mandelstam s variable is defined as

$$
\begin{aligned}
s &\equiv (p_1^\mu + p_2^\mu)^2 = (p_3^\mu + p_4^\mu)^2 \\
&= (E_1 + E_2)^2 - (\mathbf{p}_1 + \mathbf{p}_2)^2 = (E_3 + E_4)^2 - (\mathbf{p}_3 + \mathbf{p}_4)^2
\end{aligned} \tag{45}
$$

Because s is a 4-vector, then s is a relativistic invariant. The center of momentum frame is defined so that the total 3-momentum is zero,

$$\mathbf{p}_1 + \mathbf{p}_2 = 0 = \mathbf{p}_3 + \mathbf{p}_4 \qquad \text{definition of cm frame} \tag{46}$$

so that the total cm energy is

$$\sqrt{s} = E_1 + E_2 = E_3 + E_4 \equiv E_{cm} \qquad \text{in cm frame} \tag{47}$$

showing that $\sqrt{s}$ is the total energy in the cm frame.

Relation Between s and Projectile Energy in lab Frame

The lab (target) frame is defined so that the target (particle 2) is at rest,

$$\mathbf{p}_2 = 0 \qquad \text{definition of lab frame} \tag{48}$$

Thus, in the lab frame the Mandelstam invariant s is

$$
\begin{aligned}
s &= (E_1 + E_2)^2 - \mathbf{p}_1^2 \\
&= E_1^2 + 2E_1 E_2 + E_2^2 - \mathbf{p}_1^2 \\
&= m_1^2 + 2E_{1\,\text{lab}}m_2 + m_2^2
\end{aligned} \tag{49}
$$

where we have used

$$E_1 \equiv E_{1\,lab} \qquad \text{in lab frame} \tag{50}$$

and

$$E_2^2 = m_2^2 \qquad \text{in lab frame} \tag{51}$$

Note that

$$E_{1\,\text{lab}} = T_{1\,\text{lab}} + m_1 = \sqrt{\mathbf{p}_{1\,\text{lab}}^2 + m_1^2} \tag{52}$$

Threshold Energy:

Consider the reaction

$$1 + 2 \rightarrow 3 + 4 + 5 + 6 + \cdots \tag{53}$$

The Mandelstam invariant s is

$$
\begin{aligned}
s &\equiv (p_1^\mu + p_2^\mu)^2 = (p_3^\mu + p_4^\mu + p_5^\mu + p_6^\mu + \cdots)^2 \\
&= (E_1 + E_2)^2 - (\mathbf{p}_1 + \mathbf{p}_2)^2 \\
&= (E_3 + E_4 + E_5 + E_6 + \cdots)^2 - (\mathbf{p}_3 + \mathbf{p}_4 + \mathbf{p}_5 + \mathbf{p}_6 + \cdots)^2
\end{aligned} \tag{54}
$$

The particle production threshold is defined so that all the final state particles are at rest in the cm frame; that is,

$$\mathbf{p}_3 = \mathbf{p}_4 = \mathbf{p}_5 = \mathbf{p}_6 = \cdots = 0 \tag{55}$$

Thus, at threshold, the Mandelstam invariant s is

$$s = (m_3 + m_4 + m_5 + m_6 + \cdots)^2 \tag{56}$$

Because s is a relativistic invariant, we can equate it to its lab value given in equation (49), so that

$$E_{1\,\text{lab threshold}} = \frac{(m_3 + m_4 + m_5 + m_6 + \cdots)^2 - m_1^2 - m_2^2}{2m_2} \tag{57}$$

giving the threshold kinetic energy as

$$
\begin{aligned}
T_{1\,\text{lab threshold}} &= \frac{(m_3 + m_4 + m_5 + m_6 + \cdots)^2 - m_1^2 - m_2^2}{2m_2} - m_1 \\
&= \frac{(m_3 + m_4 + m_5 + m_6 + \cdots)^2 - m_1^2 - m_2^2 - 2m_1 m_2}{2m_2} \\
&= \frac{(m_3 + m_4 + m_5 + m_6 + \cdots)^2 - (m_1 + m_2)^2}{2m_2}
\end{aligned} \tag{58}
$$

14

or

$$T_{1 \text{ lab threshold}} = \frac{\left(\sum_f m_f\right)^2 - (m_1 + m_2)^2}{2m_2} \tag{59}$$

where $\sum_f m_f$ denotes the sum over the masses of all final state particles.

Speed of cm Frame

Some other useful results for the reaction $1 + 2 \to$ anything are (ref. 16)

$$\gamma = \frac{E_{1 \text{ lab}} + m_2}{\sqrt{s}} \tag{60}$$

$$\beta = \frac{\mathbf{p}_{1 \text{ lab}}}{E_{1 \text{ lab}} + m_2} \tag{61}$$

and

$$\gamma\beta = \frac{\mathbf{p}_{1 \text{ lab}}}{\sqrt{s}} \tag{62}$$

Appendix C

Maximum Pion Momentum in the cm Frame

Consider the reaction

$$A + B \rightarrow C + X \tag{63}$$

where A and B represent the projectile and target and X is anything. Using relativistic kinematics, the momentum of the C particle in the cm frame is given by (refs. 5 – 8 and 15)

$$
\begin{aligned}
\mathbf{p}^{*2}_C &= \frac{(s + m_C^2 - m_X^2)^2 - 4sm_C^2}{4s} \quad \text{as written in references (refs. 5 and 6)} \\
&= \frac{(s - m_C^2 - m_X^2)^2 - 4m_C^2 m_X^2}{4s} \quad \text{as written in references (refs. 7, 8, and 15)} \\
&= \frac{[s - (m_C + m_X)^2][s - (m_C - m_X)^2]}{4s} \tag{64}
\end{aligned}
$$

where Blattnig et al. (ref. 6) write $s_{x_{\min}}$ for m_X^2. Also, Hughes (ref. 15) writes $m_X = \sum_{i=1}^{j} m_i$ and E'^2 for s.

In determining the maximum value of $\mathbf{p}_C^2$, one demands that the X particles be produced at rest to ensure that all available momentum goes to particle C. Also, one must consider the makeup of the X particles specifically.

In previous work, pion production from proton-proton collisions was considered (refs. 5 – 8). In this reaction (with C being π),

$$p + p \rightarrow \pi + X \tag{65}$$

X must consist of at least two nucleons due to conservation of the Baryon number (ref. 9). The minimum threshold reaction is thus (ref. 9)

$$p + p \rightarrow \pi + p + p \tag{66}$$

This results (ref. 6) in $s_{x_{\min}} = m_X^2 = (m_p + m_p)^2 = 4m_p^2$, giving (refs. 5 – 8)

$$
\begin{aligned}
\mathbf{p}^{*2}_{\pi \, \max} &= \frac{(s - m_\pi^2 - 4m_p^2)^2 - 16m_\pi^2 m_p^2}{4s} \\
&= \frac{[s - (m_\pi + 2m_p)^2][s - (m_\pi - 2m_p)^2]}{4s} \quad for \quad p + p \rightarrow \pi + X \tag{67}
\end{aligned}
$$

16

For the π production reactions in the present work,

$$\pi + p \rightarrow \pi + X \tag{68}$$

Baryon number conservation requires at the least only one baryon to be produced in the final state, so that the minimum threshold reaction is (ref. 9)

$$\pi + p \rightarrow \pi + p, \tag{69}$$

which results in $m_X = m_p$. Thus, for this reaction, the maximum pion momentum is given by

$$\mathbf{p}^{*2}_{\pi \, max} = \frac{[s - (m_\pi + m_p)^2][s - (m_\pi - m_p)^2]}{4s} \qquad for \quad \pi + p \rightarrow \pi + X \tag{70}$$

For the p production reactions in the present work,

$$\pi + p \rightarrow p + X \tag{71}$$

Charge conservation requires X to have the same charge as the incident π. For strong interactions, this must also be a π so that the lowest threshold reaction is (ref. 9)

$$\pi + p \rightarrow p + \pi \tag{72}$$

Thus, $m_X = m_\pi$, which means that the maximum *proton* momentum $\mathbf{p}^*_{p \, max}$ is the *same* as the maximum pion momentum given above in (73), which is invariant under interchanging m_π and m_p. Thus,

$$\mathbf{p}^{*2}_{p \, max} = \frac{[s - (m_p + m_\pi)^2][s - (m_p - m_\pi)^2]}{4s} \qquad for \quad \pi + p \rightarrow p + X \tag{73}$$

17

Appendix D

Maximum Pion Angle in the *lab* Frame

In the cm frame, θ_π^* varies from 0 to π. Hughes (ref. 15) shows that the maximum pion angle in the lab frame is given by

$$\sin \theta_{\pi \text{ max lab}} = \sqrt{\frac{1 - V^2}{\gamma_n^2 - V^2}} \tag{74}$$

and

$$\gamma_n \equiv \frac{V}{v_\pi^*} \tag{75}$$

where $V \equiv |\mathbf{V}|$ is the speed *of* the *cm* frame and v_π^* is the speed of the pion in the *cm* frame. Therefore equation (74) becomes

$$\sin \theta_{\pi \text{ max lab}} = \sqrt{\frac{v_\pi^*}{1 - v_\pi^{*2}} \frac{1 - V^2}{V^2}} = \frac{\gamma_\pi \beta_\pi}{\gamma \beta} \tag{76}$$

where we have used $\gamma^2 \beta^2 = \frac{\beta^2}{1 - \beta^2}$ and $\gamma_\pi^2 \beta_\pi^2 = \frac{\beta_\pi^2}{1 - \beta_\pi^2}$, with $\beta \equiv V$ and $\beta_\pi^* \equiv v_\pi^*$ in units where $c = 1$. Now $\gamma_\pi \beta_\pi = |\mathbf{p}_\pi|/m_\pi$. Also, (ref. 16) combining $\beta = \frac{p_{lab}}{E_{1 lab} + m_2}$ and $\gamma = \frac{E_{1 lab} + m_2}{\sqrt{s}}$ gives $\gamma \beta = \frac{p_{lab}}{\sqrt{s}}$. Thus,

$$\sin \theta_{\pi \text{ max lab}} = \frac{\sqrt{s} \, |\mathbf{p}_\pi^*|}{|\mathbf{p}_{\text{lab}}| \, m_\pi} \tag{77}$$

In carrying out integrations over the angle, one uses $|\mathbf{p}^*_{\pi \text{ max}}|$ for $|\mathbf{p}_\pi^*|$.

This result is also the same as in references 5 and 6. (However, note that $|\mathbf{p}_{\text{lab}}|$ is denoted as p_a, and m_p incorrectly appears instead of m_π in the denominator in references 5 and 6.)

A much clearer discussion of the maximum angle is contained in reference 14. See especially the discussion on pages 402 - 403 and in figure 12.4. (The discussion occurs in the first edition (ref. 14) of this book but not in the two later editions (refs. 17 and 18).) Jackson (ref. 14) does not derive the formula of equation (77), but if one plots figure 12.4 with specific numerical values, one can see that $\theta_{\pi \text{ max}}$ in figure 12.4 gives the same numerical answer as equation (77). Figure 12.4 is simply a plot of equations (36) and (37).

Another very clear discussion of this material is in the book by Byckling (ref. 19). In the cm frame, θ_π varies from 0 to π. As Jackson (ref. 14) points out, just above threshold, α will be larger than unity, and as θ_π^* varies from 0 to π, then $\theta_\pi \equiv \theta_{\pi\,\text{lab}}$ will be confined to some forward cone $0 < \theta_\pi < \theta_{\pi\,\text{max}}$. As the incident energy rises above threshold, α will be smaller than unity and θ_π will vary all the way from 0 to π.

In the reaction $p + p \to \pi + p + p$, analyzed previously (refs. 5 and 6) one can easily calculate $\theta_{\pi\,\text{max}}$ from equation (77) or just plot the equivalent of figure 12.4 in Jackson (ref. 14). One then finds that there exists a $\theta_{\pi\,\text{max}}$ only very close to threshold. (In fact, it is less than $\frac{\pi}{2}$ near threshold.) As soon as one gets a little bit away from threshold, $\theta_{\pi\,\text{max}}$ no longer exists and therefore $\theta_\pi \equiv \theta_{\pi\,\text{lab}}$ varies from 0 to π. Given that the NASA radiation work considers pion production from threshold up to a very long way away from threshold, to all intents and purposes $\theta_{\pi\,\text{max}}$ is irrelevant, and one can simply consider that $\theta_{\pi\,\text{lab}}$ varies from 0 to π for essentially all incident energies of interest because the tiny region near threshold represents only a very tiny fraction of the energies relevant to the space radiation problem.

For the reactions $\pi + p \to \pi + p$, the threshold is zero, and it turns out that $\theta_{\pi\,\text{max}}$ never exists. For these reactions, $\theta_{\pi\,\text{lab}}$ varies from 0 to π for all incident energies of interest.

For proton production, the maximum angle is

$$\sin\theta_{p\,\text{max}} \;=\; \frac{\sqrt{s}\,|\mathbf{p}_p^*|}{|\mathbf{p}_{\text{lab}}|\,m_p} \tag{78}$$

In carrying out integrations over the angle, one uses $|\mathbf{p}_{p\,\text{max}}^*|$ for $|\mathbf{p}_p^*|$.

For proton production, the relevant reaction is $\pi + p \to p + \pi$, which has no threshold. As a result, $\theta_{p\,\text{max}}$ is also constant; however, unlike the case of pion production, this constant is exactly $\frac{\pi}{2}$. Care must be taken in numerically calculating $\theta_{p\,\text{max}}$ when using equation (78). Since $\theta_{p\,\text{max}}$ is $\frac{\pi}{2}$ when $\frac{\sqrt{s}|\mathbf{p}_p^*|}{|\mathbf{p}_{\text{lab}}|m_p} = 1$ and $\theta_{p\,\text{max}}$ is π when $\frac{\sqrt{s}|\mathbf{p}_p^*|}{|\mathbf{p}_{\text{lab}}|m_p} > 1$, the numerical round-off error can cause $\theta_{p\,\text{max}}$ to oscillate between π and $\frac{\pi}{2}$. It is recomended that any code using $\theta_{p\,\text{max}}$ put the value in explicity for the reaction $\pi + p \to p + \pi$ rather than calculating it by using equation (78).

References

1. Wilson, J. W.; Townsend, L. W.; Schimmerling, W.; Khandelwal, G. S.; Khan, F.; Nealy, J. E.; Cucinotta, F. A.; Simonsen, L. C.; Shinn, J. L.; and Norbury, J. W.: *Transport Methods and Interactions for Space Radiations.* NASA RP-1257, 1991.

2. Wilson, J. W.; Chun, S. Y.; Badavi, F. F.; Townsend, L. W.; and Lamkin, S. L.: *HZETRN: A Heavy Ion/NUcleon Transport Code for Space Radiations.* NASA TP-3146, 1991.

3. Shinn, J. L.; John, S.; Tripathi, R. K.; Wilson, J. W.; Townsend, L. W.; and Norbury, J. W.: *Fully Energy-Dependent HZETRN: A Galactic Cosmic-Ray Transport Code.* NASA TP-3243, 1992.

4. Wilson, J. W.; Badavi, F. F.; Cucinotta, F. A.; Shinn, J. L.; Badhwar, G. D.; Silberberg, R.; Tsao, C. H.; Townsend, L. W.; and Tripathi, R. K.: *HZETRN: Description of a Free-Space Ion and Nucleon Transport and Shielding Computer Program.* NASA TP-3495, 1995.

5. Blattnig, S. R.; Swaminathan, S. R.; Kruger, A. T.; Ngom, M.; and Norbury, J. W.: Parameterizations of Inclusive Cross Sections for Pion Production in Proton-Proton Collisions. *Phys. Rev. D,* vol. 62, 2000, no. 094030, pp. 1-12.

6. Blattnig, S. R.; Swaminathan, S. R.; Kruger, A. T.; Ngom, M.; Norbury, J. W.; and Tripathi, R. K.: *Paramaterized Cross Sections for Pion Production in Proton-Proton Collisions.* NASA TP-2000-210640, 2000.

7. Schneider, J. P.; Norbury, J. W.; and Cucinotta, F. A.: Parameterization of Spectral Distributions for Pion and Kaon Production in Proton-Proton Collisions. *Astrophysical Journal Supplement,* vol. 97, April 1995, pp. 571-574.

8. Schneider, J. P.; Norbury, J. W.; and Cucinotta, F. A.: *Parameterized Spectral Distributions for Meson Production in Proton-Proton Collisions.* NASA TM-4675, 1995.

9. Norbury, J. W.; Blattnig; S. R.; and Tripathi, R. K.: *Exclusive Reactions involving Pions and Nucleons.* NASA TP/2002-42512, 2002.

10. Ranft, J.: Particle Production Models Sampling High-Energy Multiparticle Events from Inclusive Single-Particle Distributions. *Computer Techniques in Radiation Transport and Dosimetry,* ed. Nelson, W. R; and Jenkins, T. M., Plenum Press, 1978.

11. Turchanovich, L. K. et al. High p_t Inclusive Hadron Production in pi- p Collisions at 40 GeV and angles $49^o \leq \theta(cm) \leq 93^o$. *Phys. Atom. Nucl.*, vol. 56, no. 10, 1993, pp. 1367-1377. Data are available at the Durham database http://durpdg.dur.ac.uk/ Accessed July 15, 2002.

12. Badhwar, G. D.; Stephens, S. A.; and Golden, R. L.: Analytic Representation of the Proton- Proton and Proton-Nucleus Cross Sections and Its Application to the Sea-Level Spectrum and Charge Ratio of Muons. *Phys. Rev. D*, vol. 15, 1977, no. 15, pp. 820-831.

13. Stephens, S. A.; and Badhwar, G. D.: Production Spectrum of Gamma Rays in Interstellar Space Through Neutral Pion Decay. *Astrophysics and Space Science*, vol. 76, 1981, pp. 213-233.

14. Jackson, J. D.: *Classical Electrodynamics*, first ed., Wiley, 1962.

15. Hughes, I. S.: *Elementary Particles*, third ed., Cambridge University Press, 1991.

16. Barnett, R. M. et al: Review of Particle Properties. *Phys. Rev. D*, vol. 54, July 1996, no. 1, pp. 1-720.

17. Jackson, J. D.: *Classical Electrodynamics*, second ed., Wiley, 1975.

18. Jackson, J. D.: *Classical Electrodynamics*, third ed., Wiley, 1999.

19. Byckling, E; and Kajantie, K.: *Particle Kinematics*. Wiley, 1973.
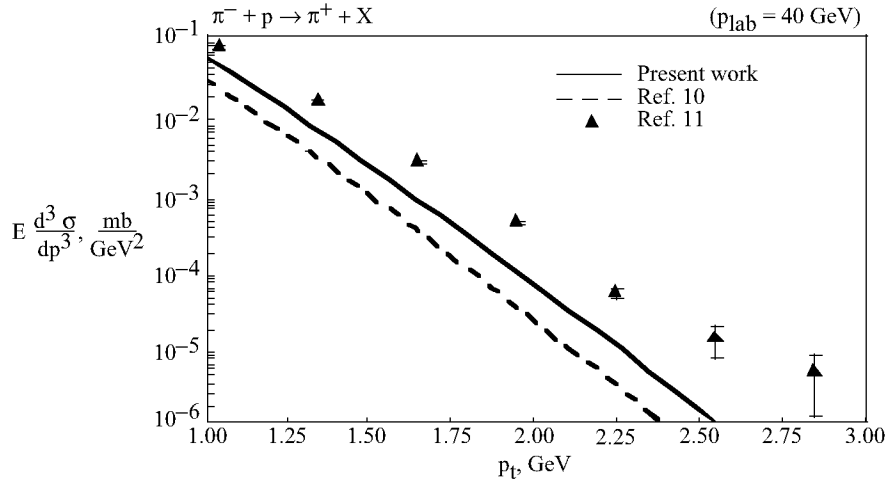
Figure 1. Lorentz invariant differential cross section $E\dfrac{d^3\sigma}{dp^3}$. The π+ is produced at $\theta_\pi^{cm} = 49°$.
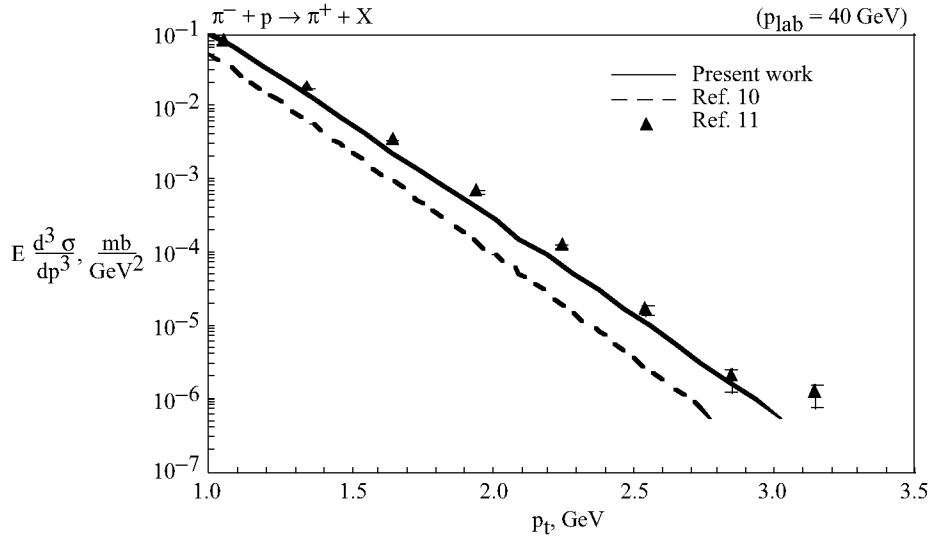
Figure 2. Lorentz invariant differential cross section $E\dfrac{d^3\sigma}{dp^3}$ for $\theta_\pi^{cm} = 62°$.
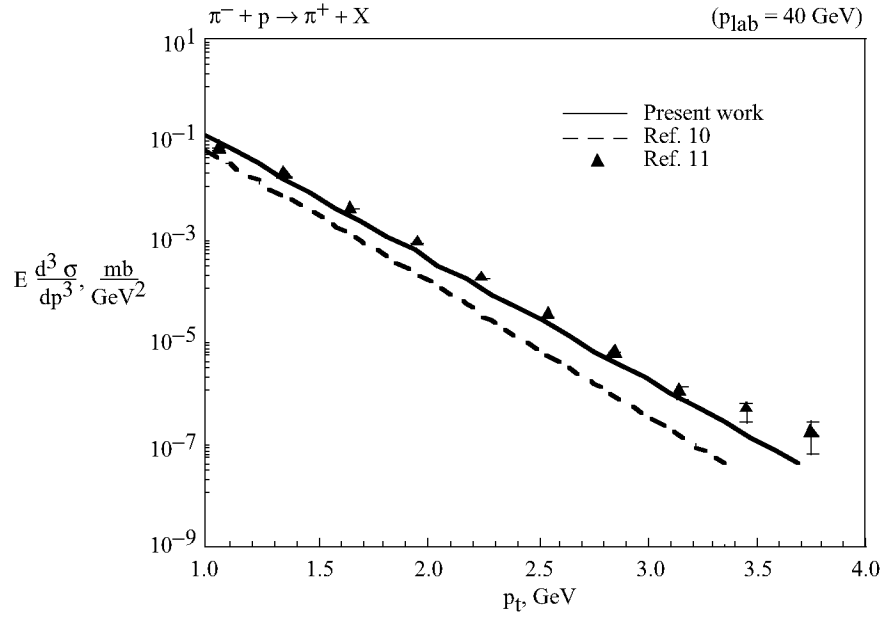
Figure 3. Lorentz invariant differential cross section $E\dfrac{d^3\sigma}{dp^3}$ for $\theta_\pi^{cm} = 73°$.
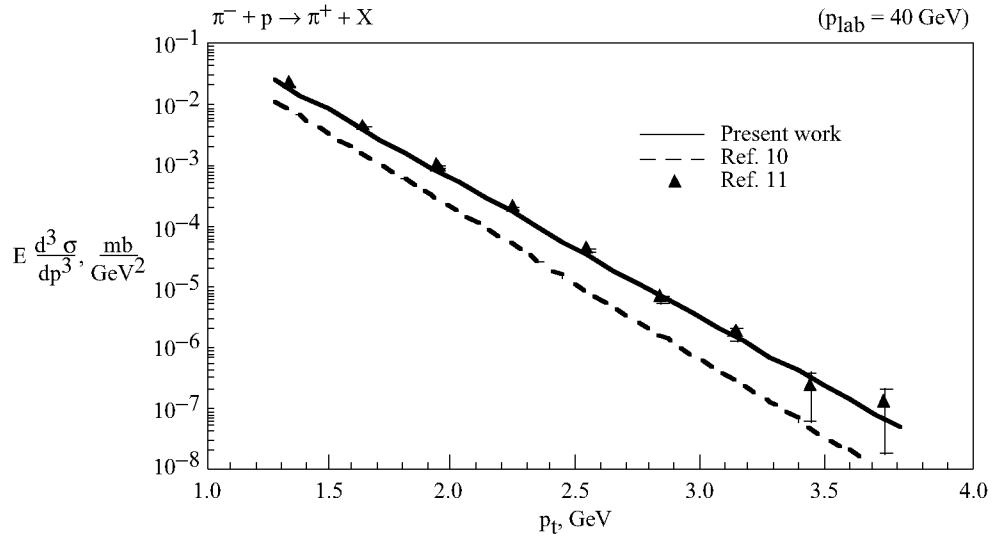
Figure 4. Lorentz invariant differential cross section $E\dfrac{d^3\sigma}{dp^3}$ for $\theta_\pi^{cm} = 83°$.

23
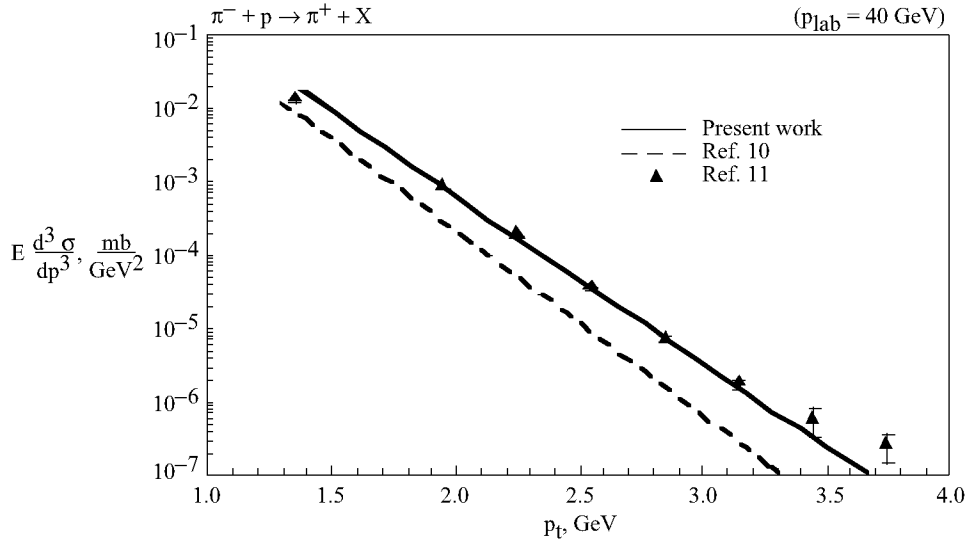
Figure 5. Lorentz invariant differential cross section $E\dfrac{d^3\sigma}{dp^3}$ for $\theta_\pi^{cm} = 93°$.
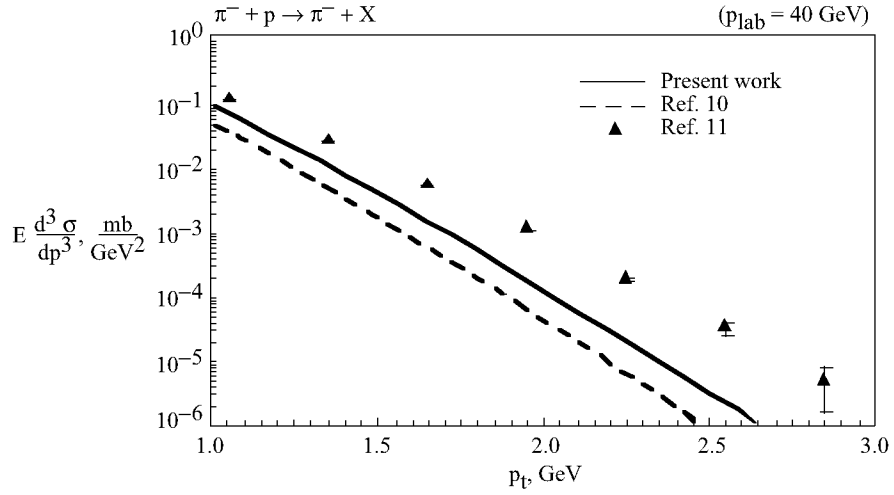
Figure 6. Lorentz invariant differential cross section $E\dfrac{d^3\sigma}{dp^3}$. The π^- is produced at $\theta_\pi^{cm} = 49°$.
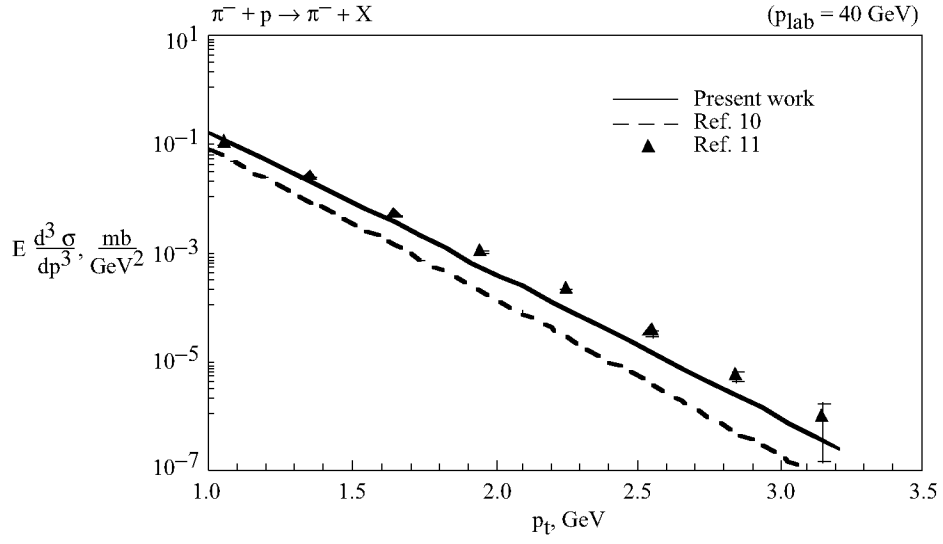
Figure 7. Lorentz invariant differential cross section $E\dfrac{d^3\sigma}{dp^3}$ for π^- at $\theta_\pi^{cm} = 62°$.
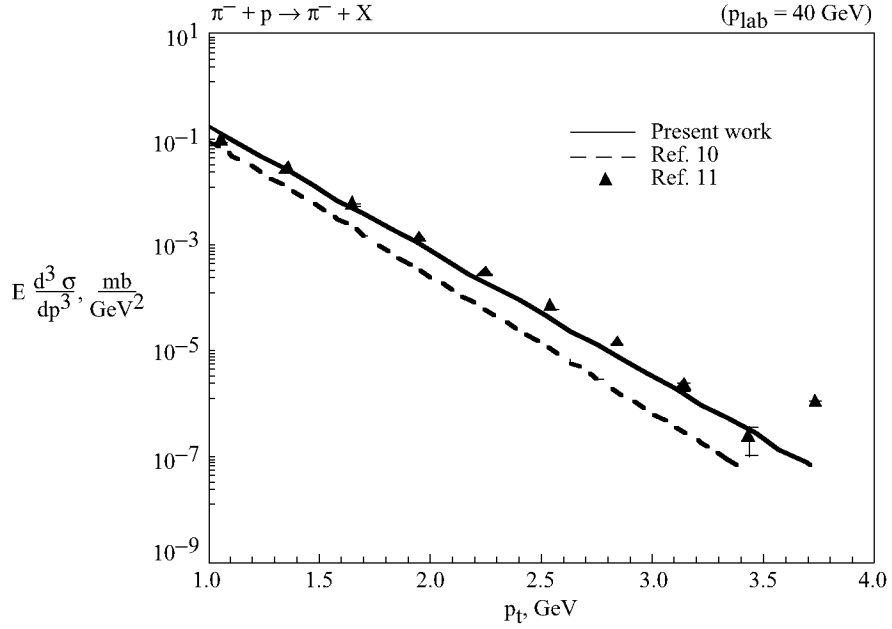
Figure 8. Lorentz invariant differential cross section for π^- at $\theta_\pi^{cm} = 73°$.
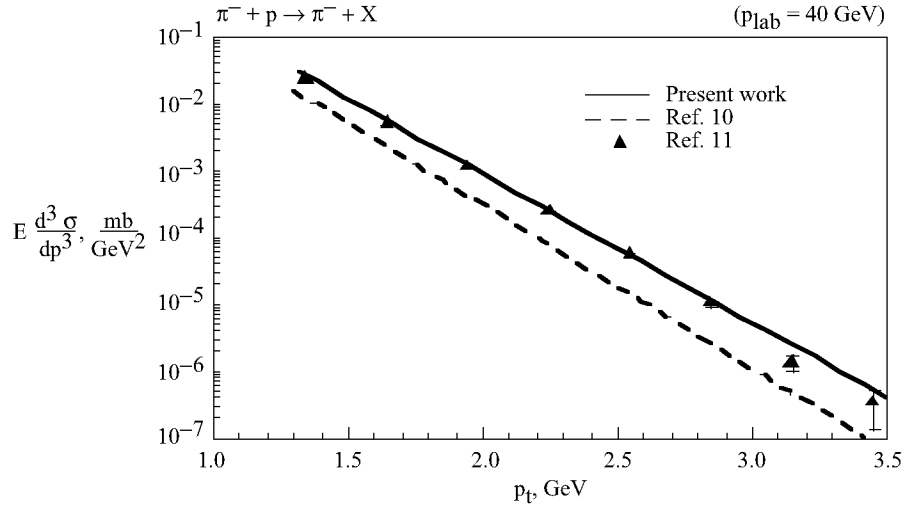
Figure 9. Lorentz invariant differential cross section $E\dfrac{d^3\sigma}{dp^3}$ for π^- at $\theta_\pi^{cm} = 83°$.
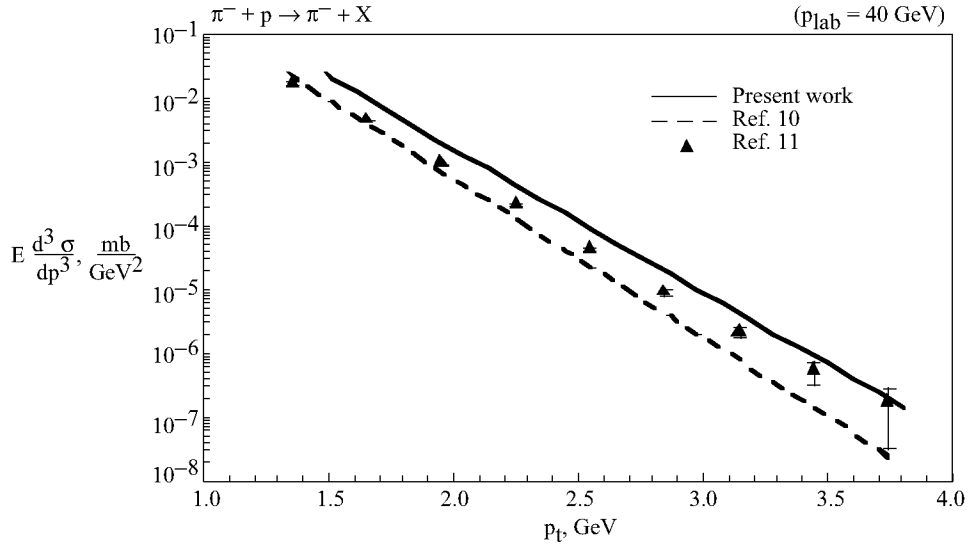
Figure 10. Lorentz invariant differential cross section $E\dfrac{d^3\sigma}{dp^3}$ for π^- at $\theta_\pi^{cm} = 93°$.

26
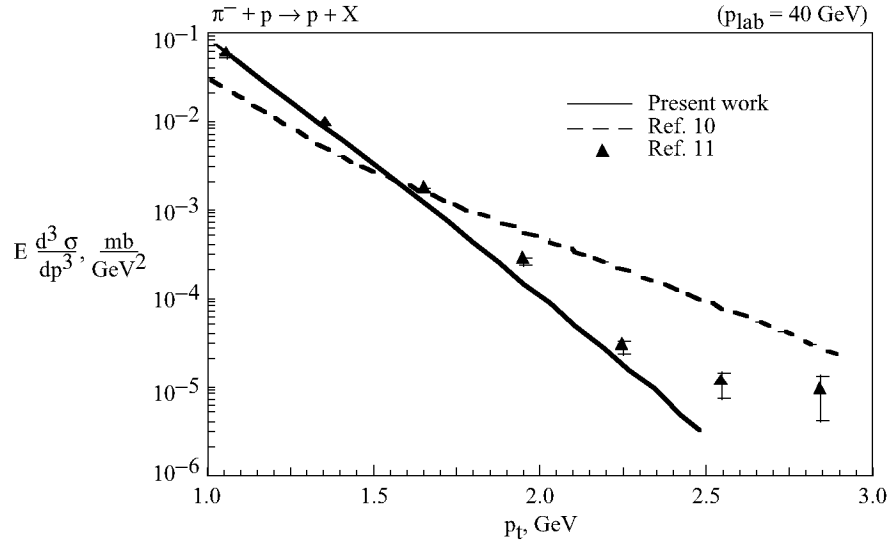
Figure 11. Lorentz invariant differential cross section $E\dfrac{d^3\sigma}{dp^3}$ for proton at $\theta_p^{cm} = 49°$.
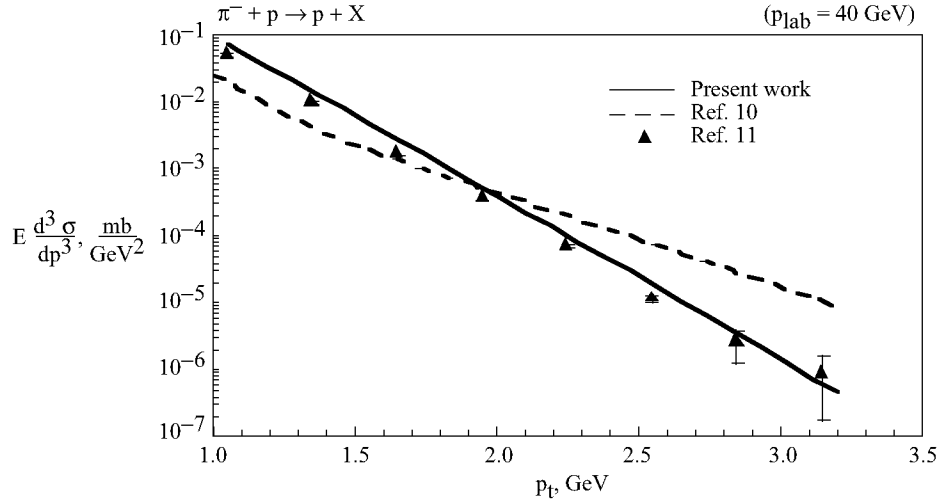
Figure 12. Lorentz invariant differential cross section $E\dfrac{d^3\sigma}{dp^3}$ for proton at $\theta_p^{cm} = 62°$.

27
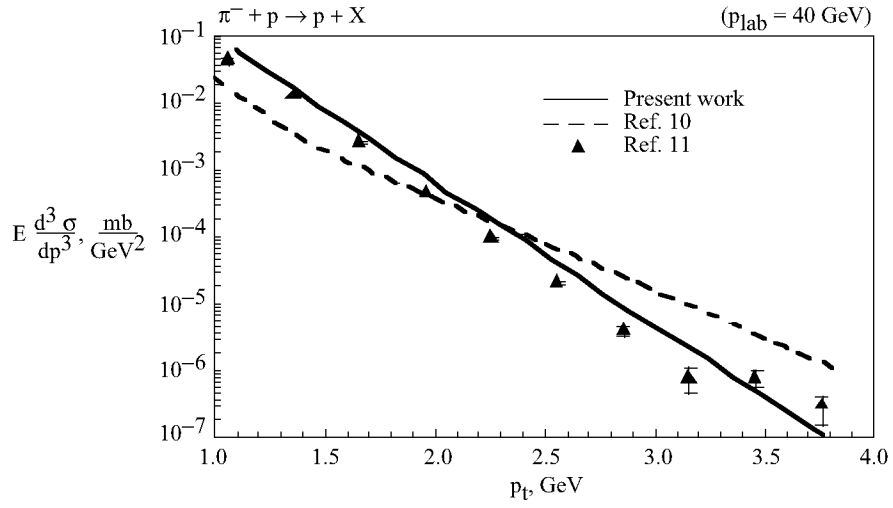
Figure 13. Lorentz invariant differential cross section $E\dfrac{d^3\sigma}{dp^3}$ for proton at $\theta_p^{cm} = 73°$.
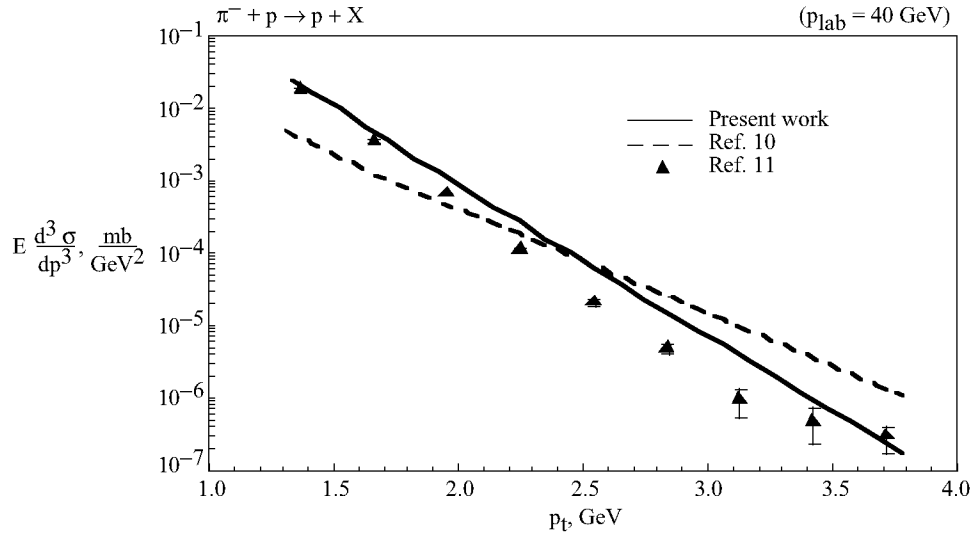
Figure 14. Lorentz invariant differential cross section $E\dfrac{d^3\sigma}{dp^3}$ for proton at $\theta_p^{cm} = 83°$.

28
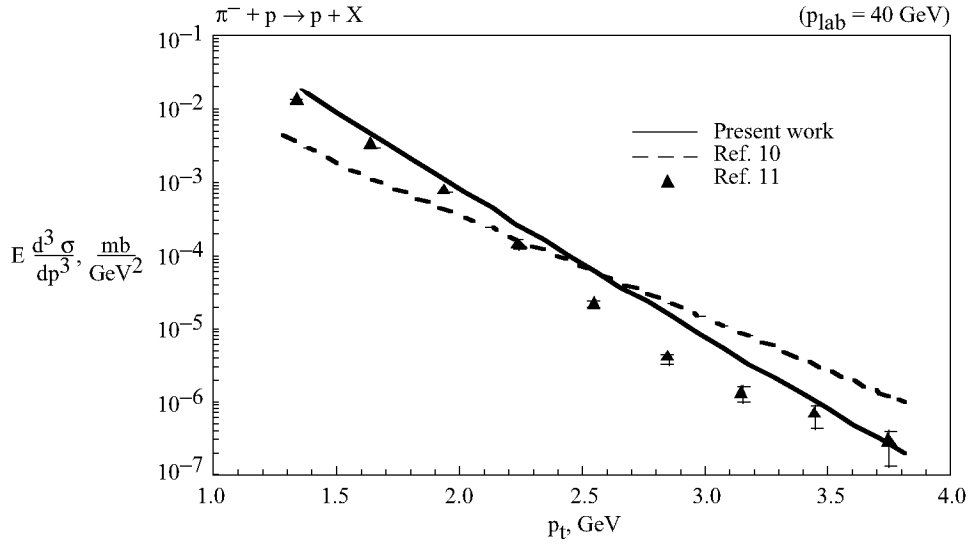
Figure 15. Lorentz invariant differential cross section $E\dfrac{d^3\sigma}{dp^3}$ for proton at $\theta_p^{cm} = 93°$.
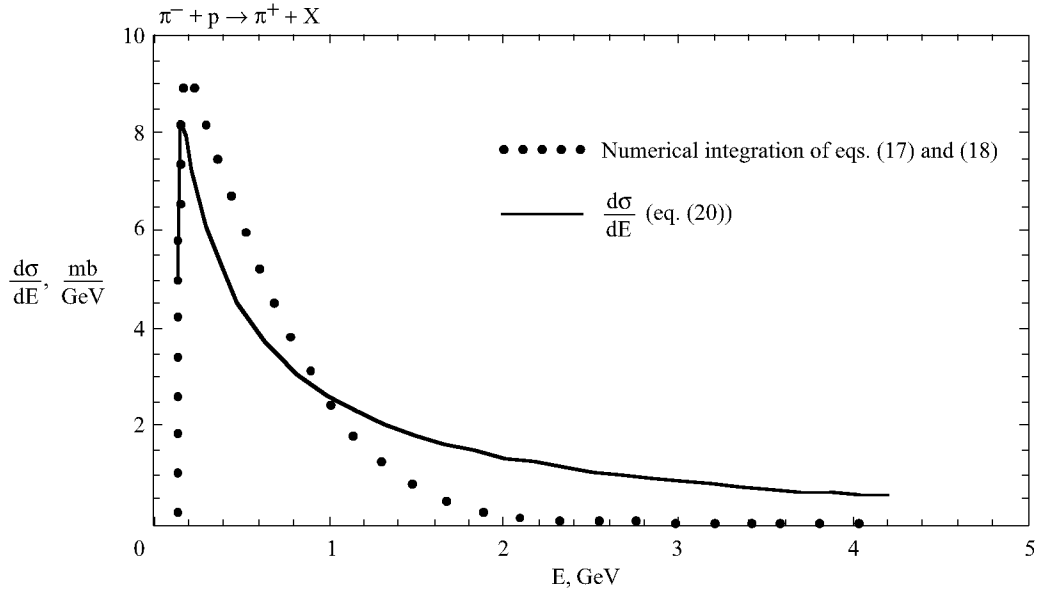
Figure 16. Parameterization of spectral distribution for π^+ production in the lab frame at $p_{1\text{ lab}} = 2$ GeV. (Note that the threshold (ref. 9) for the exclusive reaction $\pi^- + p \to \pi^+ + n + \pi^-$ is at $p_{1\text{ lab threshold}} = 279$ MeV.)
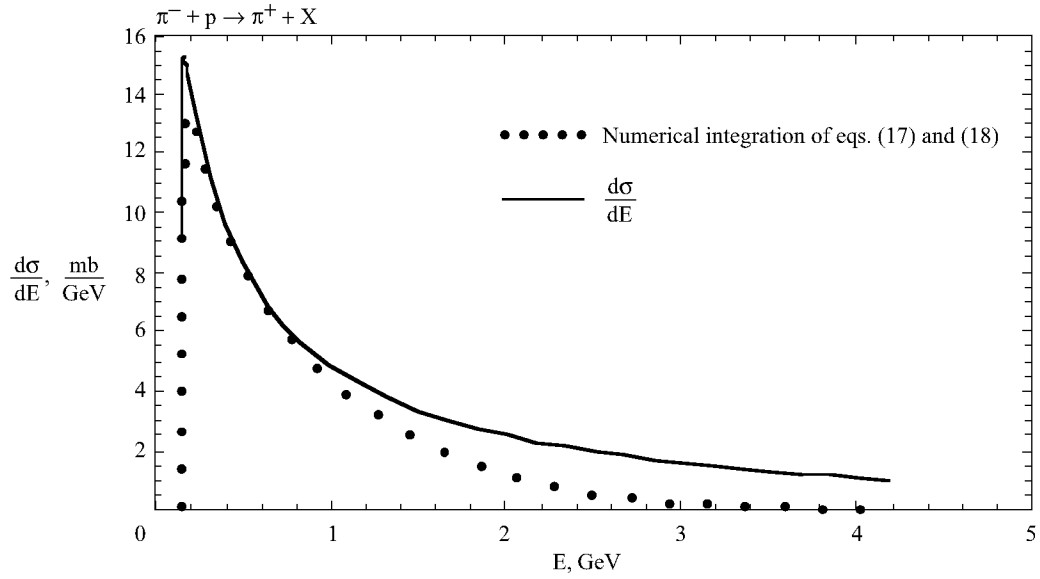
Figure 17. Parameterization of spectral distribution for π^+ production in the lab frame at $p_{1\ lab}$ = 5 GeV. (Note that the threshold (ref. 9) for the exclusive reaction $\pi^- + p \to \pi^+ + n + \pi^-$ is at $p_{1\ lab\ threshold}$ = 279 MeV.)
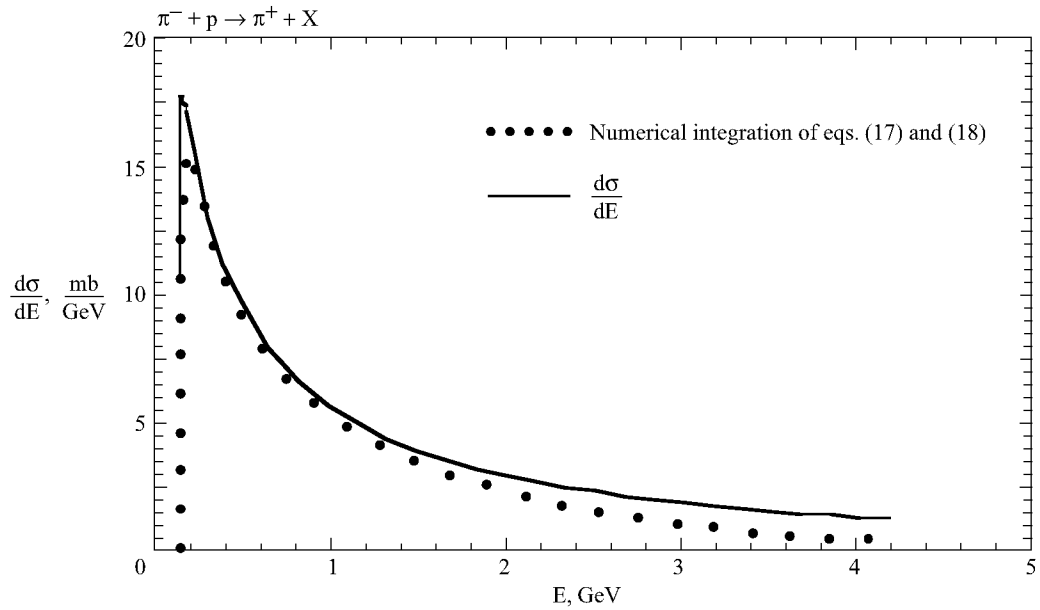
Figure 18. Parameterization of spectral distribution for π^+ production in the lab frame at $p_{1\ lab}$ = 10 GeV. (Note that the threshold (ref. 9) for the exclusive reaction $\pi^- + p \to \pi^+ + n + \pi^-$ is at $p_{1\ lab\ threshold}$ = 279 MeV.)
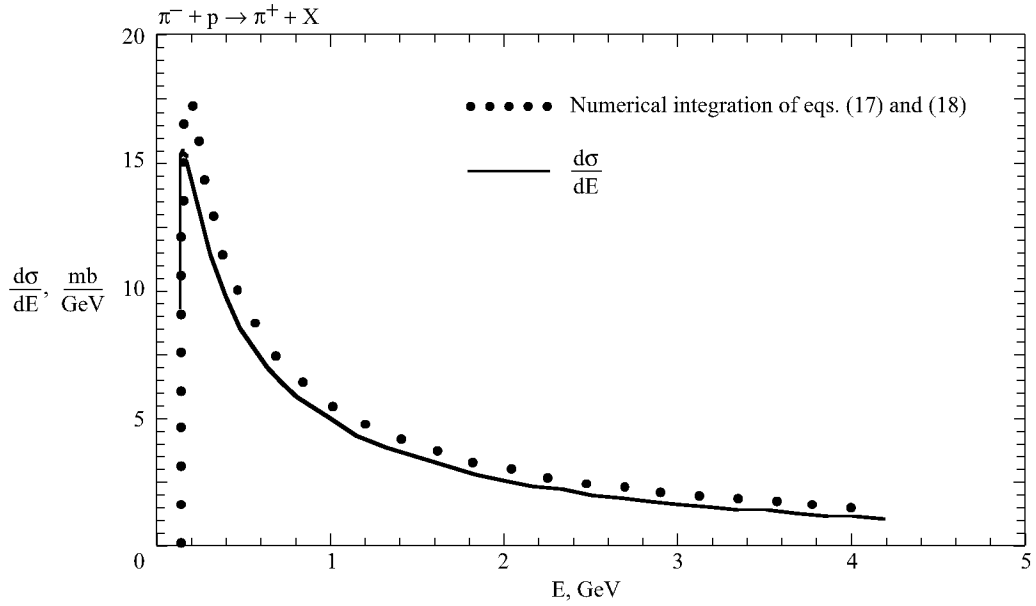
Figure 19. Parameterization of spectral distribution for π^+ production in the lab frame at $p_{1\,lab}$ = 50 GeV. (Note that the threshold (ref. 9) for the exclusive reaction $\pi^- + p \to \pi^+ + n + \pi^-$ is at $p_{1\,lab\,threshold}$ = 279 MeV.)
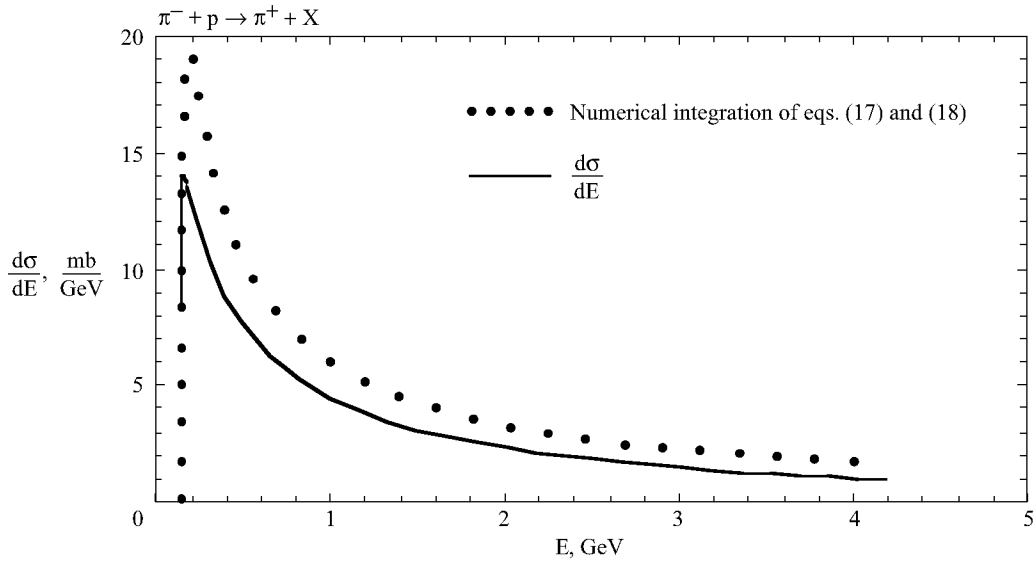
Figure 20. Parameterization of spectral distribution for π^+ production in the lab frame at $p_{1\,lab}$ = 100 GeV. (Note that the threshold (ref. 9) for the exclusive reaction $\pi^- + p \to \pi^+ + n + \pi^-$ is at $p_{1\,lab\,threshold}$ = 279 MeV.)

31
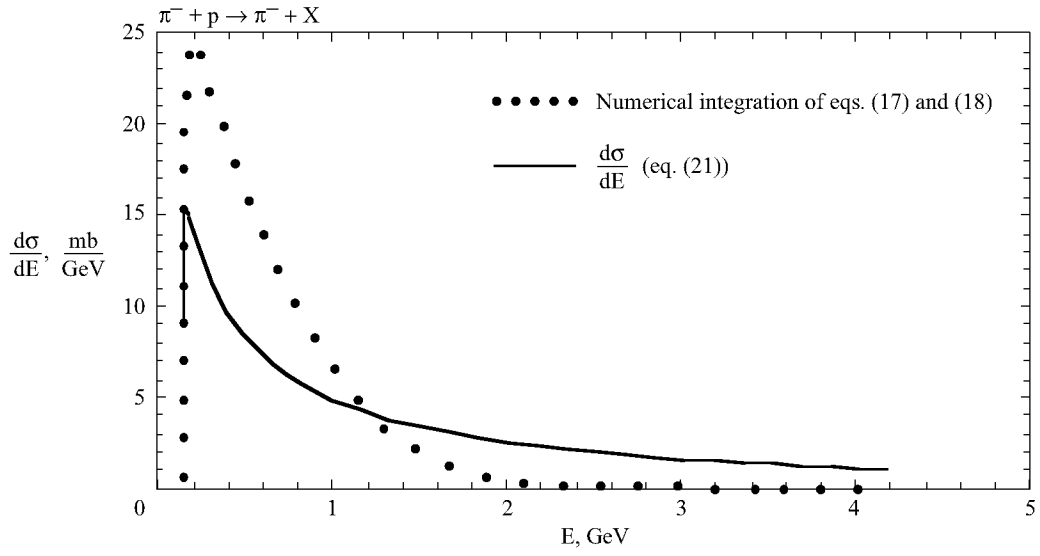
Figure 21. Parameterization of spectral distribution for π^- production in the lab frame at $p_{1\ lab}$ = 2 GeV. (Note that the threshold (ref. 9) for the exclusive reaction $\pi^- + p \rightarrow \pi^- + p$ is at $p_{1\ lab\ threshold}$ = 0.)
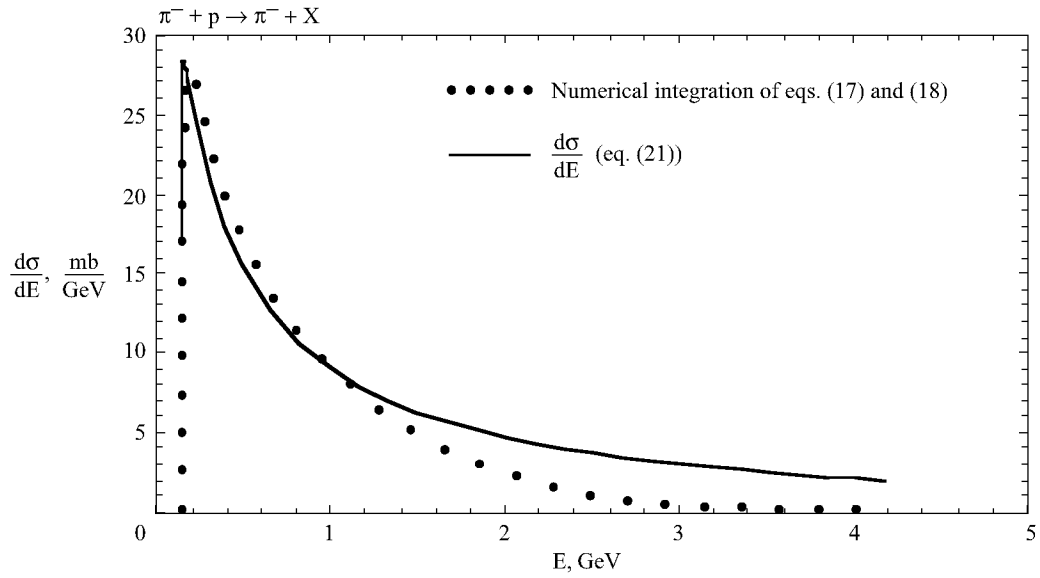

Figure 22. Parameterization of spectral distribution for π^- production in the lab frame at $p_{1\ lab}$ = 5 GeV. (Note that the threshold (ref. 9) for the exclusive reaction $\pi^- + p \rightarrow \pi^- + p$ is at $p_{1\ lab\ threshold}$ = 0.)
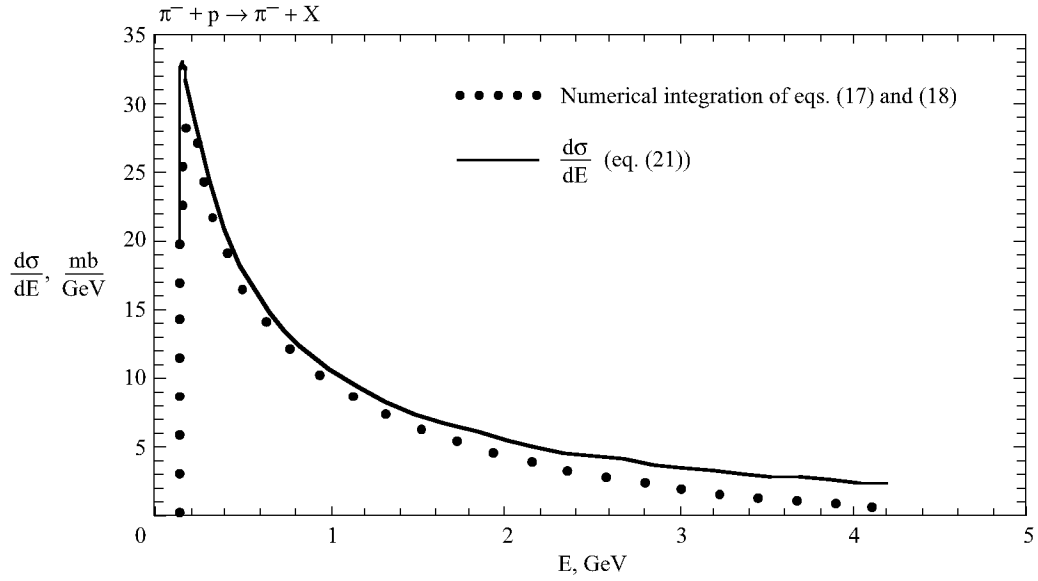
Figure 23. Parameterization of spectral distribution for π^- production in the lab frame at $p_{1\ lab} = 10$ GeV. (Note that the threshold (ref. 9) for the exclusive reaction $\pi^- + p \to \pi^- + p$ is at $p_{1\ lab\ threshold} = 0$.)
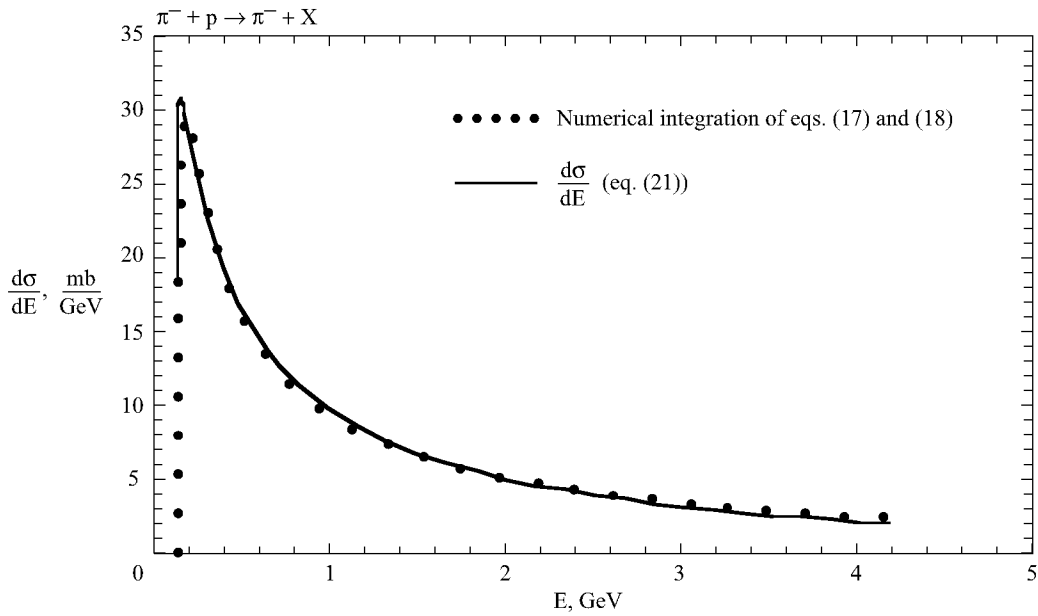
Figure 24. Parameterization of spectral distribution for π^- production in the lab frame at $p_{1\ lab} = 50$ GeV. (Note that the threshold (ref. 9) for the exclusive reaction $\pi^- + p \to \pi^- + p$ is at $p_{1\ lab\ threshold} = 0$.)
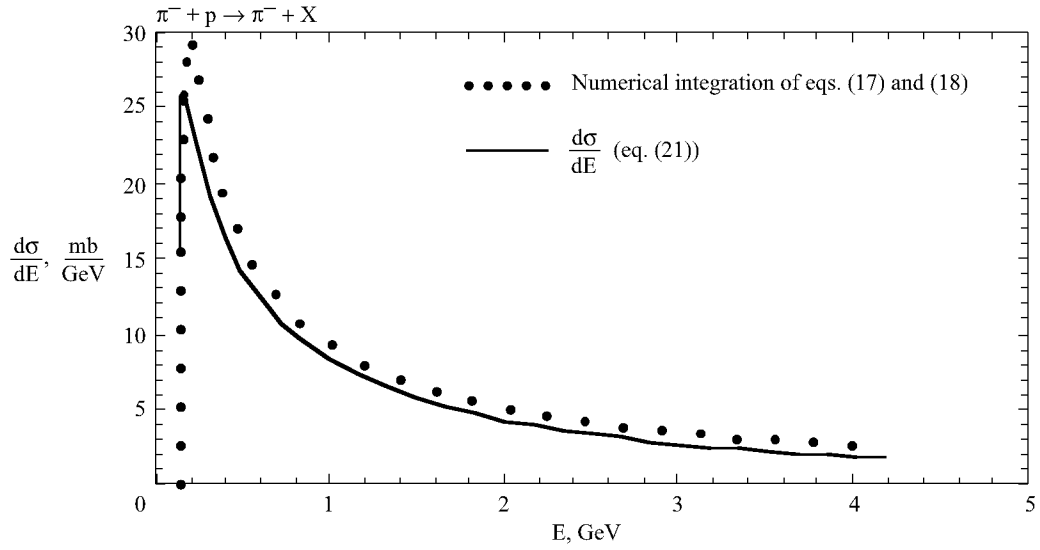
Figure 25. Parameterization of spectral distribution for π^- production in the lab frame at $p_{1\ \text{lab}} = 100$ GeV. (Note that the threshold (ref. 9) for the exclusive reaction $\pi^- + p \rightarrow \pi^- + p$ is at $p_{1\ \text{lab threshold}} = 0$.)
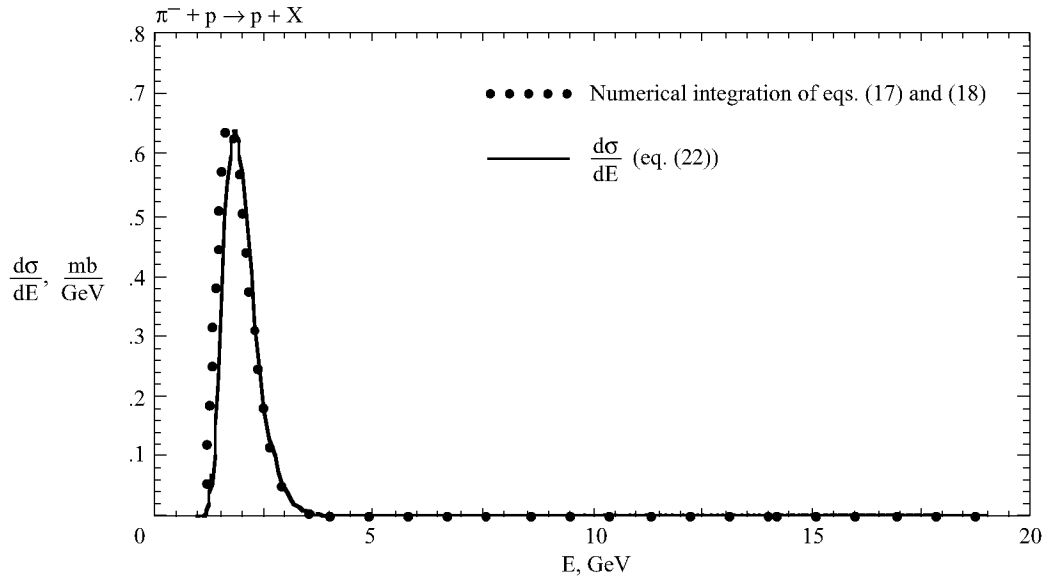

Figure 26. Fit to spectral distribution for proton production in the lab frame at $p_{1\ \text{lab}} = 2$ GeV. (Note that the threshold (ref. 9) for the exclusive reaction $\pi^- + p \rightarrow \pi^- + p$ is at $p_{1\ \text{lab threshold}} = 0$.)
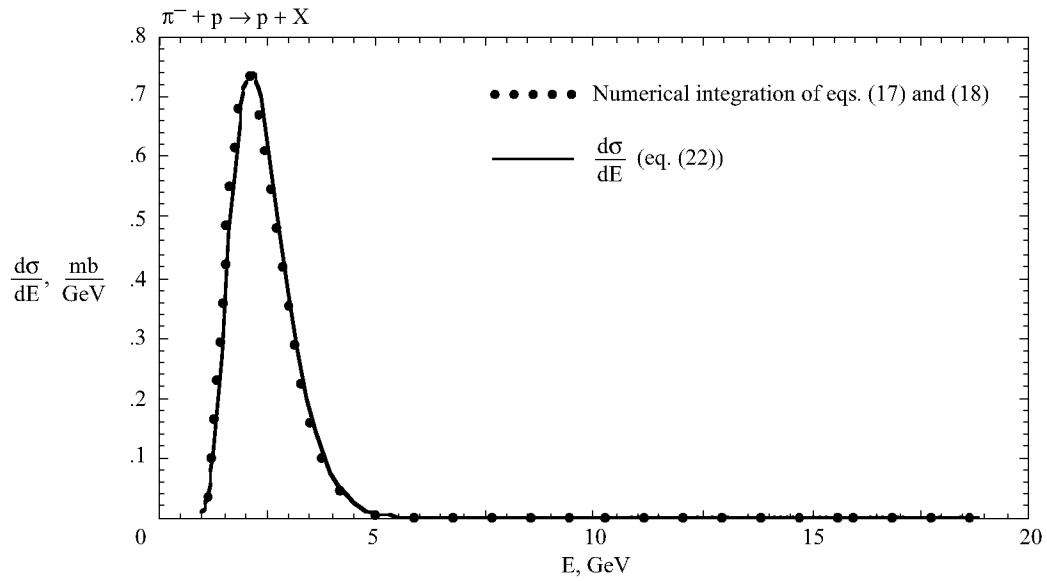
Figure 27. Fit to spectral distribution for proton production in the lab frame at $p_{1\ \text{lab}}$ = 5 GeV. (Note that the threshold (ref. 9) for the exclusive reaction $\pi^- + p \rightarrow p + \pi^-$ is at $p_{1\ \text{lab threshold}} = 0$.)
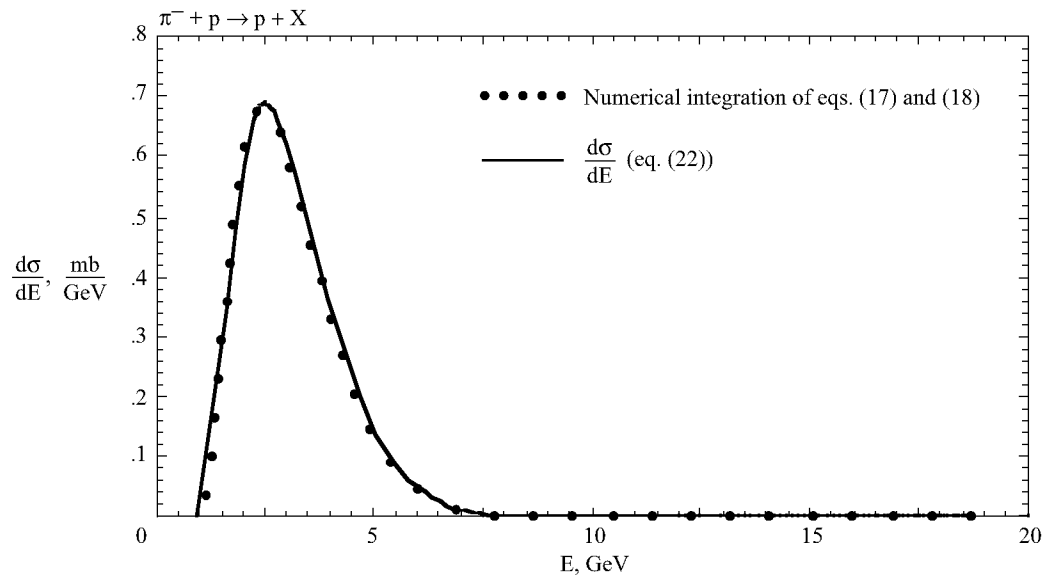
Figure 28. Fit to spectral distribution for proton production in the lab frame at $p_{1\ \text{lab}}$ = 10 GeV. (Note that the threshold (ref. 9) for the exclusive reaction $\pi^- + p \rightarrow p + \pi^-$ is at $p_{1\ \text{lab threshold}} = 0$.)
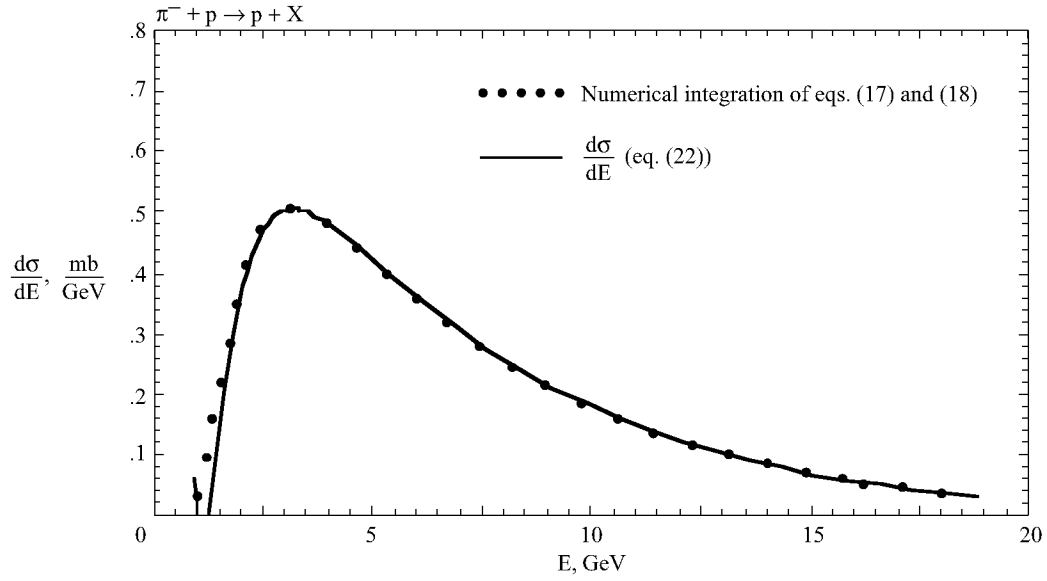
Figure 29. Fit to spectral distribution for proton production in the lab frame at $p_{1\ lab}$ = 50 GeV. (Note that the threshold (ref. 9) for the exclusive reaction $\pi^- + p \to p + \pi^-$ is at $p_{1\ lab\ threshold}$ = 0.)
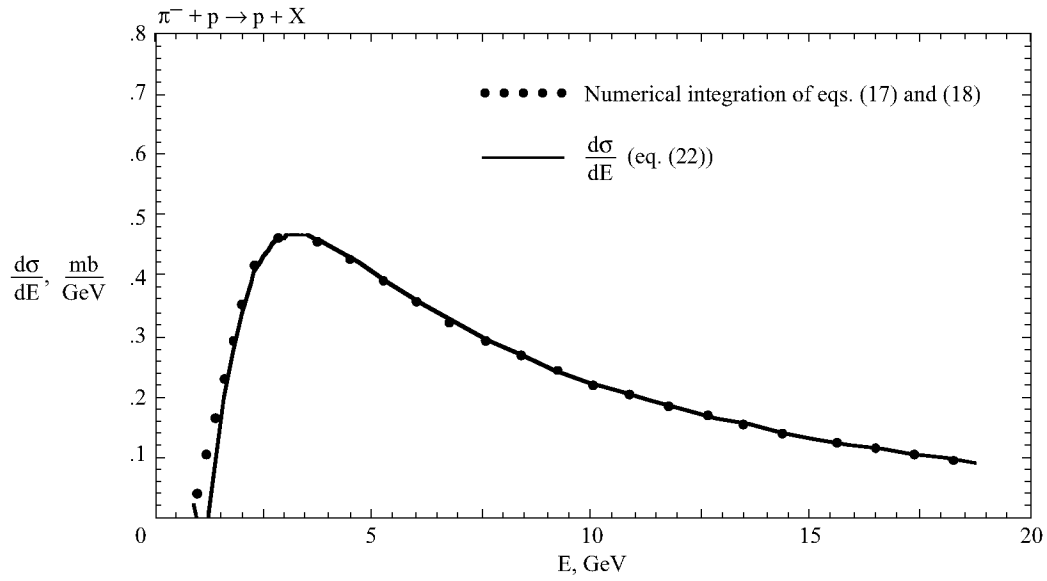
Figure 30. Fit to spectral distribution for proton production in the lab frame at $p_{1\ lab}$ = 100 GeV. (Note that the threshold (ref. 9) for the exclusive reaction $\pi^- + p \to p + \pi^-$ is at $p_{1\ lab\ threshold}$ = 0.)

36
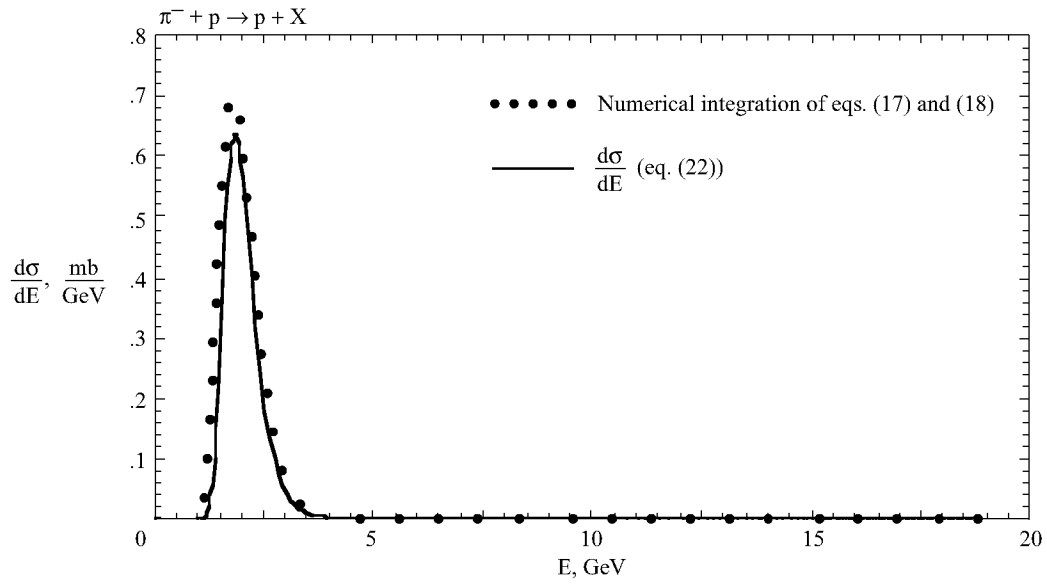
Figure 31. Parameterization of spectral distribution for proton production in the lab frame at $p_{1\,lab}$ = 2.5 GeV.
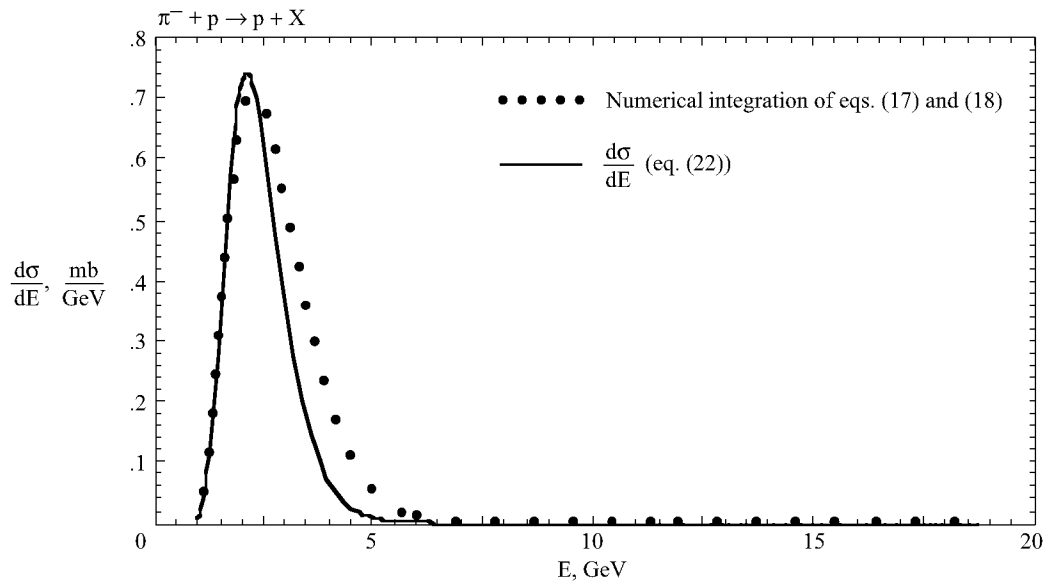
Figure 32. Parameterization of spectral distribution for proton production in the lab frame at $p_{1\,lab}$ = 7.5 GeV.

37
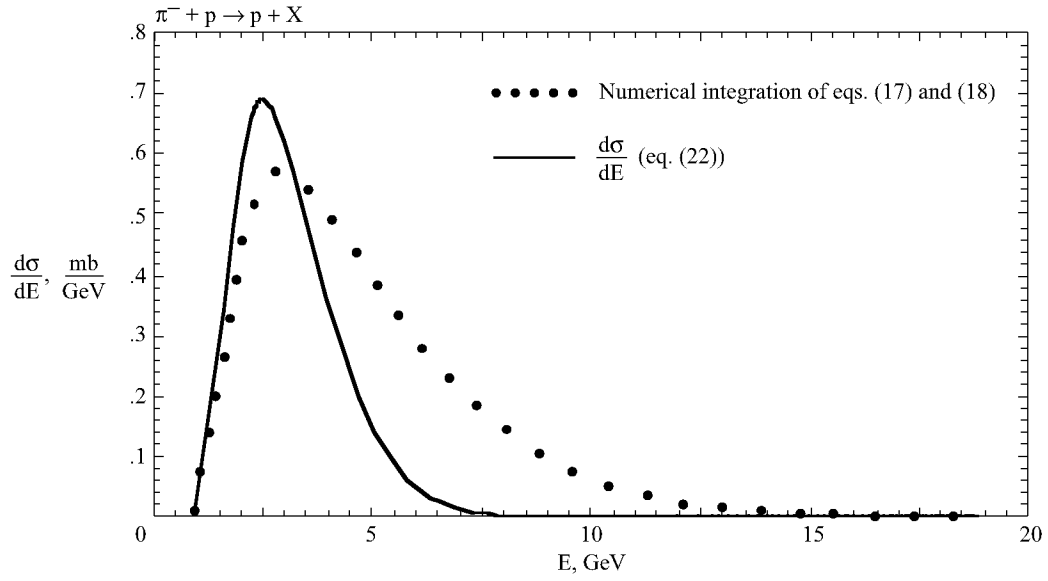
Figure 33. Parameterization of spectral distribution in the lab frame at $p_{1\,lab} = 25$ GeV.
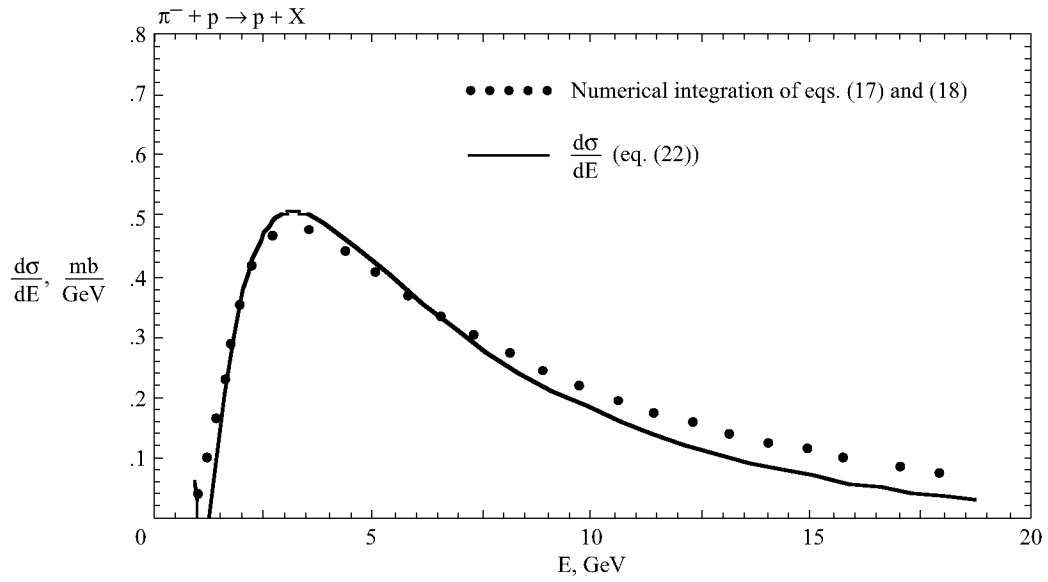
Figure 34. Parameterization of spectral distribution for proton production in the lab frame at $p_{1\,lab} = 75$ GeV.
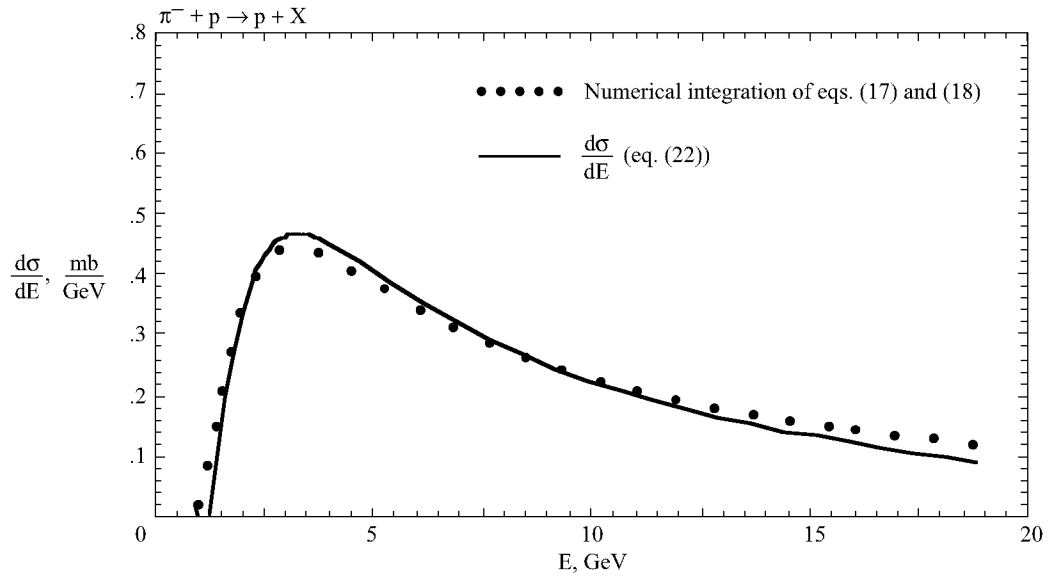
Figure 35. Parameterization of spectral distribution in the lab frame at $p_{1\,lab}$ = 200 GeV.
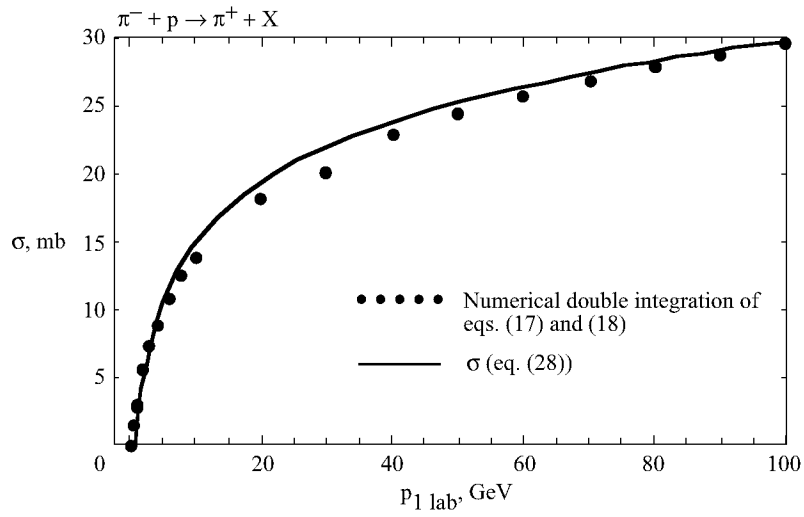
Figure 36. Parameterization of total cross section for π^+ production (eq. (28)).

$\pi^- + p \rightarrow \pi^- + X$

Numerical double integration of eqs. (17) and (18)

σ (eq. (29))
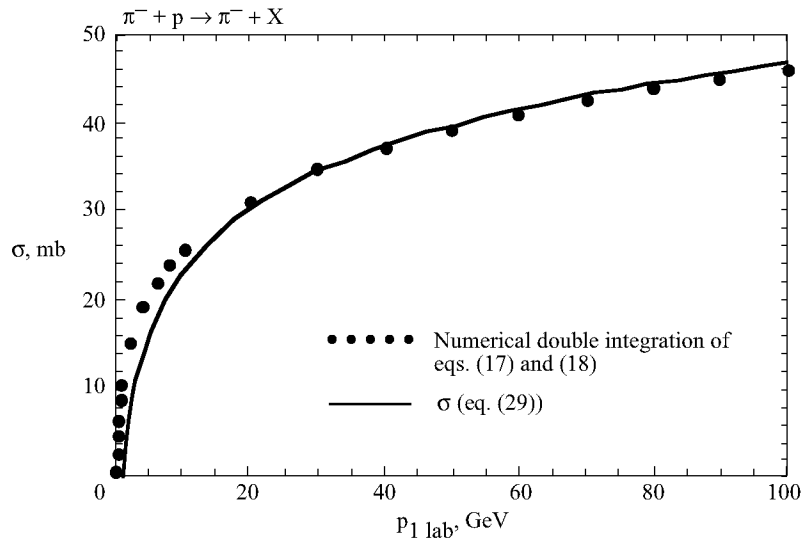
Figure 37. Parameterization of total cross section for π^- production (eq. (29)).

$\pi^- + p \rightarrow p + X$

Numerical double integration of eqs. (17) and (18)

σ (eq. (30))

Figure 38. Parameterization of total cross section for proton production (eq. (30)).

40

REPORT DOCUMENTATION PAGE

1. REPORT DATE *(DD-MM-YYYY)*	2. REPORT TYPE	3. DATES COVERED *(From - To)*
12-2002	Technical Paper	

4. TITLE AND SUBTITLE

Cross-Section Parameterizations for Pion and Nucleon Production From Negative Pion-Proton Collisions

5a. CONTRACT NUMBER

5b. GRANT NUMBER

5c. PROGRAM ELEMENT NUMBER

6. AUTHOR(S)

Norbury, John W.; Blattnig, Steve R.; Norman, Ryan; and Tripathi, R. K.

5d. PROJECT NUMBER

5e. TASK NUMBER

5f. WORK UNIT NUMBER
755-06-00-03

7. PERFORMING ORGANIZATION NAME(S) AND ADDRESS(ES)

NASA Langley Research Center
Hampton, VA 23681-2199

8. PERFORMING ORGANIZATION REPORT NUMBER

L-18210

9. SPONSORING/MONITORING AGENCY NAME(S) AND ADDRESS(ES)

National Aeronautics and Space Administration
Washington, DC 20546-0001

10. SPONSOR/MONITOR'S ACRONYM(S)

NASA

11. SPONSOR/MONITOR'S REPORT NUMBER(S)

NASA/TP-2002-211766

12. DISTRIBUTION/AVAILABILITY STATEMENT

Unclassified - Unlimited
Subject Category 93
Availability: NASA CASI (301) 621-0390   Distribution: Standard

13. SUPPLEMENTARY NOTES

Norbury, Blattnig, and Norman: University of Wisconsin-Milwaukee, Milwaukee, WI; and Tripathi: Langley Research Center, Hampton, VA
An electronic version can be found at http://techreports.larc.nasa.gov/ltrs/ or http://techreports.larc.nasa.gov/cgi-bin/NTRS

14. ABSTRACT

Ranft has provided parameterizations of Lorentz invariant differential cross sections for pion and nucleon production in pion-proton collisions that are compared to some recent data. The Ranft parameterizations are then numerically integrated to form spectral and total cross sections. These numerical integrations are further parameterized to provide formula for spectral and total cross sections suitable for use in radiation transport codes. The reactions analyzed are for charged pions in the initial state and both charged and neutral pions in the final state.

15. SUBJECT TERMS

Negative pion-proton collisions; Parameterization of differential, spectral, and total cross sections; Interaction transport codes; Comparison with Ranft parameterization

16. SECURITY CLASSIFICATION OF:			17. LIMITATION OF ABSTRACT	18. NUMBER OF PAGES	19a. NAME OF RESPONSIBLE PERSON
a. REPORT	b. ABSTRACT	c. THIS PAGE			STI Help Desk (email: help@sti.nasa.gov)
U	U	U	UL	46	19b. TELEPHONE NUMBER *(Include area code)* (301) 621-0390